NAVAL POSTGRADUATE SCHOOL

MONTEREY, CALIFORNIA

THESIS

APPLICATION OF TIME-REVERSAL MIRROR TO PASSIVE REMOTE SENSING OF THE OCEAN

by

Dexter Y. Tan

June 2021

Thesis Advisor: Oleg A. Godin
Co-Advisor: Derek Olson

THIS PAGE INTENTIONALLY LEFT BLANK

REPORT DOCUMENTATION PAGE			Form Approved OMB No. 0704-0188

1. AGENCY USE ONLY *(Leave blank)*	**2. REPORT DATE** June 2021	**3. REPORT TYPE AND DATES COVERED** Master's thesis

4. TITLE AND SUBTITLE
APPLICATION OF TIME-REVERSAL MIRROR TO PASSIVE REMOTE SENSING OF THE OCEAN

5. FUNDING NUMBERS
RPLG4

6. AUTHOR(S) Dexter Y. Tan

7. PERFORMING ORGANIZATION NAME(S) AND ADDRESS(ES)
Naval Postgraduate School
Monterey, CA 93943-5000

8. PERFORMING ORGANIZATION REPORT NUMBER

9. SPONSORING / MONITORING AGENCY NAME(S) AND ADDRESS(ES)
National Science Foundation (Arlington, VA 22314)

10. SPONSORING / MONITORING AGENCY REPORT NUMBER

11. SUPPLEMENTARY NOTES The views expressed in this thesis are those of the author and do not reflect the official policy or position of the Department of Defense or the U.S. Government.

12a. DISTRIBUTION / AVAILABILITY STATEMENT
Approved for public release. Distribution is unlimited.

12b. DISTRIBUTION CODE
A

13. ABSTRACT (maximum 200 words)

Characterizing the underwater environment can be approached directly by taking measurements, or by inversion where geoacoustic properties of the environment are derived from the way sound interacts with it. Single-element time-reversal mirror was proposed as a physics-motivated, data processing technique, utilizing inputs from either a controlled source or noise interferometry. Once completed, the same technique can be used to detect and track quiet underwater targets, maximizing naval application by allowing surreptitious monitoring, especially in denied areas, with single receivers that are easier to deploy than arrays.

Solving the inverse problem with this technique results in ambiguous solutions, however. When a single metric of spatial focus is used, multiple combinations of geoacoustic parameters are able to meet the criteria set. In this work, we propose and evaluate additional metrics, based on temporal focus expected from the time-reversal mirror process, to evaluate the different combinations and arrive at the unique solution, with parameters that match the environment. Using numerical simulations, in the cases examined, this was achieved with a subset of the proposed metrics, thereafter applied in a specific sequence, to arrive at the unique solution.

Having completed analysis via numerical simulations, our recipe of metrics is ready to be assessed with real-world data.

14. SUBJECT TERMS acoustic noise interferometry, time reversal mirror	**15. NUMBER OF PAGES** 75
	16. PRICE CODE

17. SECURITY CLASSIFICATION OF REPORT	**18. SECURITY CLASSIFICATION OF THIS PAGE**	**19. SECURITY CLASSIFICATION OF ABSTRACT**	**20. LIMITATION OF ABSTRACT**
Unclassified	Unclassified	Unclassified	UU

NSN 7540-01-280-5500

Standard Form 298 (Rev. 2-89)
Prescribed by ANSI Std. 239-18

THIS PAGE INTENTIONALLY LEFT BLANK

Approved for public release. Distribution is unlimited.

APPLICATION OF TIME-REVERSAL MIRROR TO PASSIVE REMOTE SENSING OF THE OCEAN

Dexter Y. Tan
Major, Republic of Singapore Navy
B Ch E, National University of Singapore, 2009

Submitted in partial fulfillment of the
requirements for the degree of

MASTER OF SCIENCE IN PHYSICAL OCEANOGRAPHY

from the

NAVAL POSTGRADUATE SCHOOL
June 2021

Approved by: Oleg A. Godin
Advisor

Derek Olson
Co-Advisor

Peter C. Chu
Chair, Department of Oceanography

THIS PAGE INTENTIONALLY LEFT BLANK

ABSTRACT

Characterizing the underwater environment can be approached directly by taking measurements or by inversion, where geoacoustic properties of the environment are derived from the way sound interacts with it. Single-element time-reversal mirror was proposed as a physics-motivated, data processing technique, utilizing inputs from either a controlled source or noise interferometry. Once completed, the same technique can be used to detect and track quiet underwater targets, maximizing naval application by allowing surreptitious monitoring, especially in denied areas, with single receivers that are easier to deploy than arrays.

Solving the inverse problem with this technique results in ambiguous solutions, however. When a single metric of spatial focus is used, multiple combinations of geoacoustic parameters are able to meet the criteria set. In this work, we propose and evaluate additional metrics, based on temporal focus expected from the time-reversal mirror process, to evaluate the different combinations and arrive at the unique solution, with parameters that match the environment. Using numerical simulations, in the cases examined, this was achieved with a subset of the proposed metrics, thereafter applied in a specific sequence, to arrive at the unique solution.

Having completed analysis via numerical simulations, our recipe of metrics is ready to be assessed with real-world data.

THIS PAGE INTENTIONALLY LEFT BLANK

TABLE OF CONTENTS

LIST OF FIGURES

LIST OF TABLES

LIST OF ACRONYMS AND ABBREVIATIONS

PE	Parabolic Equation
PM	peak magnitude of the time-reversal mirror-processed signal
PT	time when the peak of the time-reversal mirror-processed signal occurs
RAM	parabolic equation-based, finite-difference Range-Dependent Acoustic Model
RD	range discrepancy between time-reversal mirror-processed spatial focus and true location
SNR	signal-to-noise ratio
SR	symmetry ratio of the time-reversal mirror-processed signal
TRM	time-reversal mirror
TWHH	time width of the time-reversal mirror-processed signal at half the height of the main peak

THIS PAGE INTENTIONALLY LEFT BLANK

ACKNOWLEDGMENTS

First and foremost, I thank my advisor, Dr. Oleg Godin, for his trust and faith in my choice of research, given my inexperience and lack of background knowledge in the chosen field. His guidance and patience were most crucial in my journey.

Many thanks are extended to my second advisor, Dr. Derek Olson, without whom I would not have been able to overcome the coding challenges I faced, with my minimal prior MATLAB experience. His guidance helped me to understand the field of underwater acoustics and made the steep learning curve easier to scale.

LCDR Tsu Wei Tan of the Republic of China Navy, who, even though he had completed his doctorate the quarter I began my NPS journey, provided the stepping stones for me.

Exchange students from the French Naval Academy, then-EV2 Renucci Thomas and then-EV2 Voyer Antoine, provided the initial direction of my research from their prior work.

Last but not least, and most importantly, I thank my wife, Xinni, and our two beautiful boys, Coen and Callen, who dropped everything they were familiar with and travelled across the world with me. To greet parenthood in an unfamiliar environment, surrounded by unfamiliar people, was definitely not an easy step to take, but without them, I would not have been able to complete this endeavor.

THIS PAGE INTENTIONALLY LEFT BLANK

I. INTRODUCTION

A. THE UNDERWATER ENVIRONMENT

Understanding the battlespace is fundamental in warfare as it allows us to exploit the natural environment, as well as to avoid disadvantages. In the maritime above-water warfare environment, sensors primarily use electromagnetic waves for detection and tracking. Unfortunately, their high attenuation underwater limits their use to short ranges. Underwater, acoustic waves reign supreme.

B. SOLVING THE INVERSE PROBLEM

Low frequency acoustic wave propagation in the ocean is affected predominantly by sound speed in the water column and geoacoustic parameters of the seabed. The former can be calculated using measurements of temperature, salinity, and pressure, by way of sensors such as bathythermographs and Conductivity, Temperature, and Depth sensors. More arduous to measure are the parameters concerning the sea floor, comprising one or more layers of varying materials, each with their own geoacoustic properties, such as sound speed and density. Water column and seabed parameters are necessary in order to model the acoustic propagation environment, whether for campaign planning purposes, to predict sonar detection ranges and performance, or to anticipate locations of shadow zones.

This approach begins with environmental parameters and ends with understanding how sound waves propagate underwater. The inverse problem, as the name suggests, begins at the opposite end and uses acoustic propagation to retrieve the environmental parameters. While this method requires computational resources to obtain the desired information, it reduces the need for sensors and challenging procedures, such as retrieving sea floor samples, some from thousands of meters below the surface. Contact methods are also not able to provide the spatial resolution required for accurate representation.

C. THESIS ORGANIZATION

The remainder of this thesis first details relevant background and theory in Chapter II, as well as introducing the problem of ambiguous solution that our research aims to

address. In Chapter III, we introduce metrics that form the basis of our methodology to solve this problem. Chapter IV presents our tests, evaluations, and analysis of the efficacy of our methodology in various underwater environments. Chapter V wraps up our research with conclusions drawn as well as recommendations for future study.

II. BACKGROUND AND THEORY

A. ACOUSTIC REMOTE SENSING

Described by Dowling and Sabra in 2015 [1], as acoustic waves travel through a medium, in this case the ocean, they carry information from both their source and the environment via the routes taken. Analyzing them can provide valuable insights into their source and the environment along the paths that the waves travelled. In a waveguide bounded by the water surface above and the sea floor below, multiple paths traversed by these waves cover almost the entire water column, between the source and receivers. Figure 1 shows a generic underwater acoustic remote sensing scenario and the various processes affecting the waves.

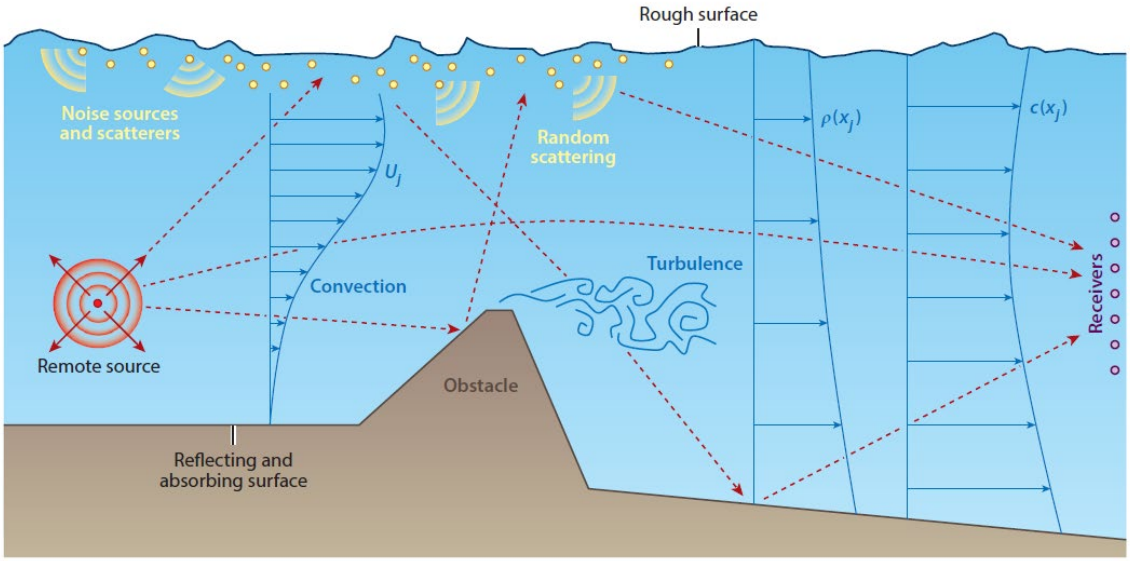

Figure 1. Underwater Acoustic Remote Sensing scenario. Source: [1].

At the destination (made up of one or more receivers), sound is analyzed to extract the relevant information. These sounds can comprise known or unknown origins, like a source or ambient noise from shipping and marine life in the ocean. Acoustic remote sensing is categorized into four broad functions [1]:

1. Detection, or determining if a source is present
2. Localization, or finding spatially where a source is
3. Source signal recovery, or reconstructing the original waveform
4. Environmental characterization, or determining one or more parameters of the environment

Our research focuses on the aforementioned fourth task, which can be further broken down into two categories: (1) making use of a known source, with information such as location and transmitted signal, and (2) leveraging ambient noise recorded at the same time but at spatially different positions in the ocean.

B. TIME-REVERSAL MIRROR

Time-reversal mirror (TRM) traditionally refers to the process of utilizing an array of receivers to detect signals in the forward propagation, reversing them in time and transmitting using backward propagation to focus the signal both spatially and temporally. This process is based on waves being reciprocal in a stationary medium, where they propagate and take equivalent routes even if the source and receiver are interchanged [2]. Parvulescu and Clay first demonstrated temporal focus in 1965 [3], followed by Kuperman et. al exemplifying the full spatial and temporal focusing of a TRM in the ocean in 1998, using vertical arrays or acoustic transceivers [4]. TRM was illustrated as a physical process, where a pulse from a transponder was transmitted to a vertical source-receiver array, digitized, and retransmitted to a vertical receiver array collocated with the transponder. More recently, TRM can also be numerically simulated, making it a physics-motivated processing technique. The time-reversal and back propagation steps are conducted numerically, and with the correct environmental parameters, a focus would be obtained with properties similar to observations in field experiments. If the parameters are incorrect, the focus may not occur, be positioned at a different location, or may not have characteristics that are expected.

For the purpose of characterizing the environment, in order to obtain the acoustic field, the input for the TRM process can be from a compact, controlled source, or equivalent

data can be retrieved using noise interferometry from cross correlation of signals received at two points. While the latter input inherently results in a more challenging process, the benefit of being able to surreptitiously complete the TRM process and characterize the underwater environment would be greatly advantageous.

In 2017, Godin et al. investigated a new approach to passive acoustic remote sensing of the ocean, combining noise interferometry and the TRM concept to solve the inverse problem in the absence of a known source. Single receivers were also positioned spatially apart at two points as compared to a vertical array, further differentiating from earlier studies [5].

TRM foci are usually poorly defined unless back-propagated waves converge at the focus from different directions. To improve accuracy, multiple paths taken by the signal are consequently desired. Using an array of receivers, the geometry of the ocean environment becomes less of a factor as received signals from multiple paths can be obtained. In a shallow water environment, where the range-to-depth ratio is large, path diversity can also be obtained by leveraging reflections off the surface and bottom in the waveguide.

In the first part of their range-independent studies, using numerical simulations, Godin et al. were able to retrieve estimates of the unknown physical parameters of the waveguide (bottom sound speed and density ratio) in a shallow water, homogeneous, fluid bottom half space. They also demonstrated the possibility of obtaining a robust focus using a single-element TRM and acoustically characterized the seabed in the model, where the unknown geoacoustic parameters were thickness of a sediment layer, sediment sound speed and density, and sub-bottom sound speed and density. Thereafter, in the second part of their study, they applied this new technique to data from the Florida Strait noise interferometry experiment in 2012, obtaining geoacoustic parameter values consistent with those evaluated via other independent methods.

Qin et al. conducted further research in 2017 using the same approach to solve the inverse problem with noise interferometry and TRM, applying the techniques to data from the Shallow Water 2006 experiment, conducted off the New Jersey coast [6]. They

considered the range-dependent environment and successfully estimated the sound speed and density ratio of a homogeneous, fluid bottom half space. In the aforementioned two studies, the criterion used to find the true solution of the inverse problem, matching geoacoustic parameters, was correct geometric position of the focus. It was subsequently realized that a problem of ambiguity in the solutions occurs when a finer grid search is utilized, or when a wider range of geoacoustic parameters are allowed to compete. This issue of ambiguous solutions will be further expounded later in this chapter.

Subsequently, in his 2019 Naval Postgraduate School thesis, McMullin further examined this issue of ambiguity, also using data from the Shallow Water 2006 experiment [7]. McMullin attempted to resolve the ambiguity in the solutions from noise interferometry and TRM by studying the feasibility of three metrics to characterize the TRM focus. He discovered that in the simplified environmental model of a coastal ocean considered, the metrics studied individually yielded different sets of possible solutions. When combined and analyzed together, the metrics could be used to identify the true solution.

The goal of this work is to explore other, more widely applicable, ways to resolve these ambiguous solutions to the inverse problem of characterizing the acoustic environment in a littoral ocean, using the concept of a single-element TRM.

C. PARABOLIC EQUATION AND RANGE-DEPENDENT ACOUSTIC MODEL

We modelled our environments' acoustical fields using the Parabolic Equation (PE) approximation, which was first developed for electromagnetic wave propagations, then adapted for acoustic waves [8]. Specifically, we utilized Dzieciuch's MATLAB package [9] that was adapted from the finite-element approach Range-Dependent Acoustic Model (RAM) developed by Collins [10].

PE, and RAM in particular, compute the underwater acoustic field by marching in range and calculating the acoustical pressure at all points between the source and receiver. In this manner, we modelled the forward propagation of our source signal, receiving it at the receiver. The received signal is then reversed in time, which is equivalent to complex

conjugation in the frequency domain, and back propagated in the environment as the TRM signal. The focus obtained from this back propagation would indicate the estimated source's position, which is dependent on the geoacoustic parameters inputted [5].

1. Application of TRM Processing to Models with Homogeneous Fluid Bottom

In order to verify that our code was accurate, we first attempted to reproduce the numerical simulations of a single-element acoustic TRM in a shallow water waveguide with a homogeneous fluid bottom from [5]. Four models present different ranges between source and receiver and source signal bandwidths. Across the four models, common geoacoustic parameters are as follows in Table 1, and differing parameters are in Table 2.

Table 1. Common parameters in homogeneous fluid bottom models

Depth of water	100 m
Depth of source and receiver	95 m
Bottom sound speed, c_b	1750 m/s
Bottom density ratio, ρ_b (relative to the density of water)	1.9
Bottom attenuation, α_b (λ is the wavelength of sound)	0.3 dB/λ

Table 2. Differing parameters in homogeneous fluid bottom models

Panel (a) Range from source to receiver: 5015 m Source signal frequency: 20–200 Hz	**Panel (b)** Range from source to receiver: 5015 m Source signal frequency: 20–70 Hz
Panel (c) Range from source to receiver: 9760 m Source signal frequency: 20–200 Hz	**Panel (d)** Range from source to receiver: 9760 m Source signal frequency: 20–70 Hz

Reproduced in Figure 2, from [5], are the results of the four models, where the normalized peak intensities of the back-propagated acoustic field are shown in the vertical cross section of the waveguide, depicting the TRM focus. The white circle represents the source position.

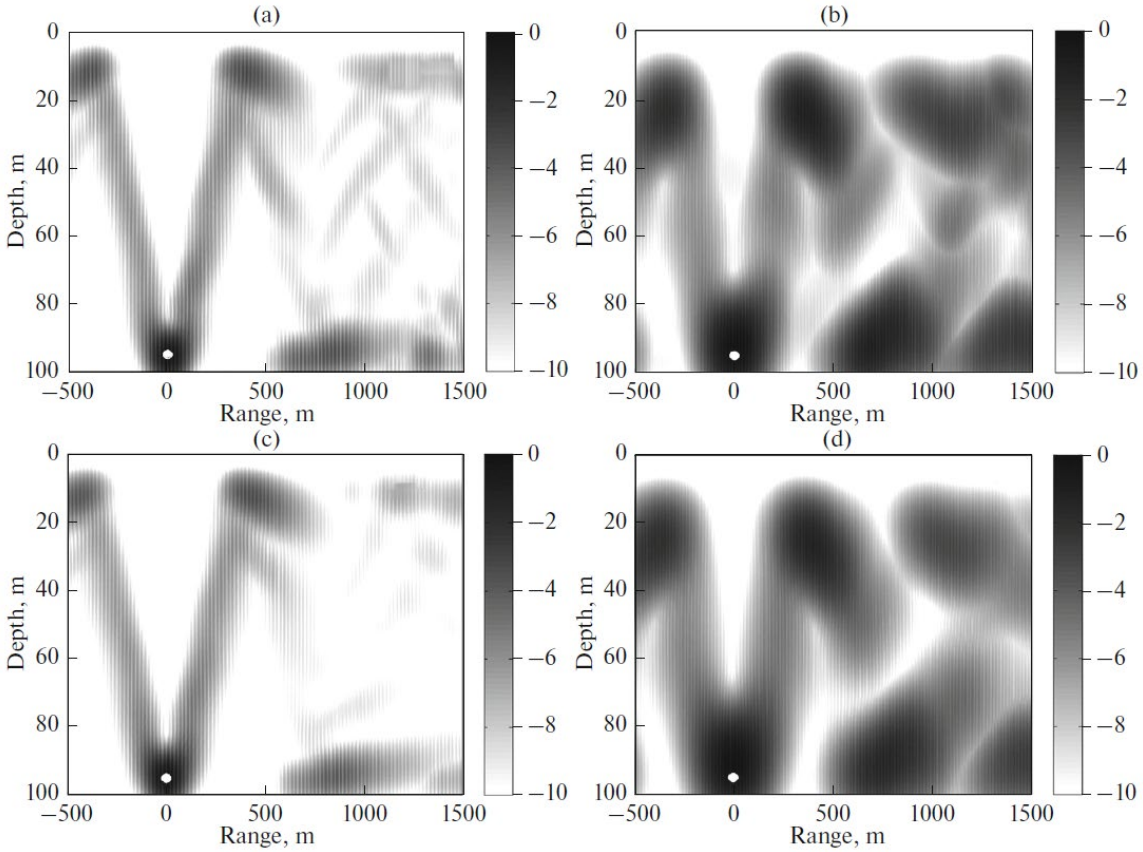

(a) 5015 m range, 20–200 Hz signal; (b) 5015 m range, 20–70 Hz signal; (c) 9760 m range, 20–200 Hz signal; (c) 9760m range, 20–70 Hz signal.

Figure 2. Numerical simulations of a single-element TRM in homogeneous fluid bottom models. Source: [5].

Utilizing our code, we reproduced these four models, presented in Figure 3. We also calculated the horizontal range difference between the TRM focus and the source position.

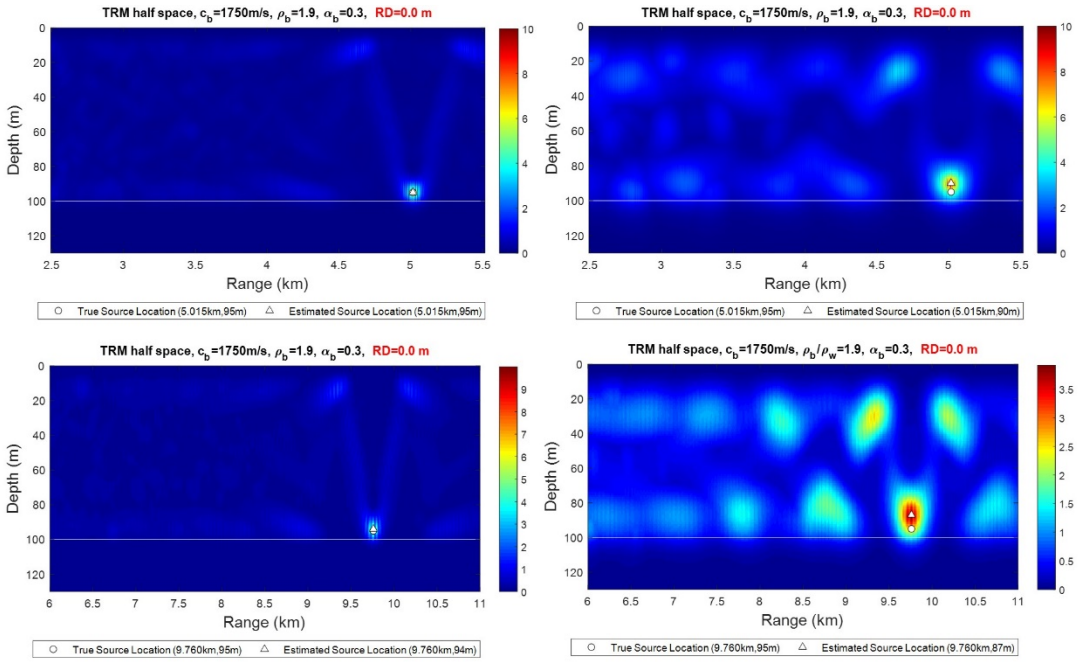

(Top-left) 5015 m range, 20–200 Hz signal; (Top-right) 5015 m range, 20–70 Hz signal; (Bottom-left) 9760 m range, 20–200 Hz signal; (Bottom-right) 9760m range, 20–70 Hz signal.

Figure 3. Reproduced numerical simulations of a single-element TRM in homogeneous fluid bottom models

The plots are similar, and with the calculated ranges we were able to determine that the TRM foci matched up with the source position horizontally. In our plot, the range dimension (along the x-axis) represented the range of the TRM focus away from the receiver as we examined the backward propagation. This was in contrast to the original results, where the plots showed range as an absolute, with 0 m where the source was and 5015 m (or 9760 m) where the receiver was.

2. Application of TRM Processing to Models with Sediment Layer Seabed

Next, we attempted to reproduce the numerical simulations of a single-element TRM in a seabed with sediment layer waveguide from [5]. Above the homogeneous fluid bottom, we added a sediment layer with a specific thickness, sound speed, and density. Here, the intent was to display the effects that these additional geoacoustic parameters had

on the TRM focus of the back propagation. Common parameters of the waveguide are in Table 3, and differing parameters are in Table 4.

Table 3. Common parameters in seabed with sediment layer models

Depth of water	100 m
Depth of source and receiver	95 m
Range from source to receiver	5015 m
Source signal bandwidth	20–70 Hz
Sediment thickness, H	20 m
Sediment attenuation, α_b (λ is the wavelength of sound)	0.1 dB/λ
Bottom sound speed, c_b	1800 m/s
Bottom density ratio, ρ_b (relative to the density of water)	2.2
Bottom attenuation, α_b (λ is the wavelength of sound)	0.1 dB/λ

Table 4. Differing parameters in seabed with sediment layer models

Panel (a) Sediment sound speed c_s: 1550 m/s Sediment density ratio, ρ_s: 1.3	
Panel (b) Sediment sound speed c_s: 1540 m/s Sediment density ratio, ρ_s: 1.3	**Panel (c)** Sediment sound speed c_s: 1560 m/s Sediment density ratio, ρ_s: 1.3
Panel (d) Sediment sound speed c_s: 1550 m/s Sediment density ratio, ρ_s: 1.2	**Panel (e)** Sediment sound speed c_s: 1550 m/s Sediment density ratio, ρ_s: 1.4

Figure 4, reproduced from [5], shows the five different seafloor models with the control environment in panel (a). Panels (b) and (c) altered sediment sound speed lower and higher, respectively, and plotted the calculated TRM focus against the source position. Panels (d) and (e) presented changes for sediment density ratio similarly.

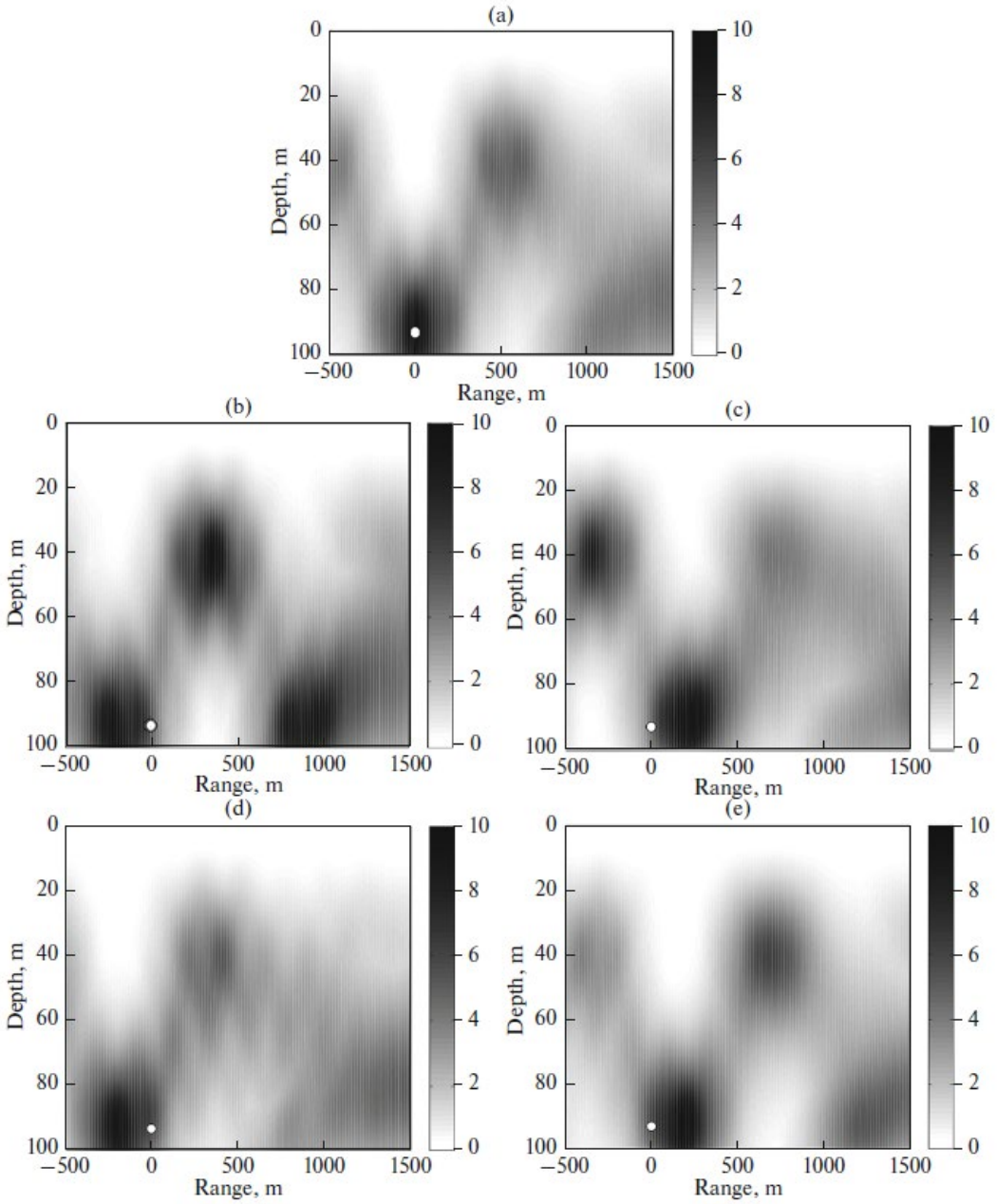

The sediment sound speed c_s and density ratio ρ_s are: (a) 1550 m/s and 1.3; (b) 1540 m/s and 1.3; (c) 1560 m/s and 1.3; (d) 1550 m/s and 1.2; (e) 1550 m/s and 1.4.

Figure 4. Effects of mismatched geoacoustic parameters on TRM focus. Source: [5].

Figure 5 shows our reproduction of the models showing the effects of mismatched geoacoustic parameters on the TRM focus, and a glimpse of the sensitivity that the parameters have on the position of the foci.

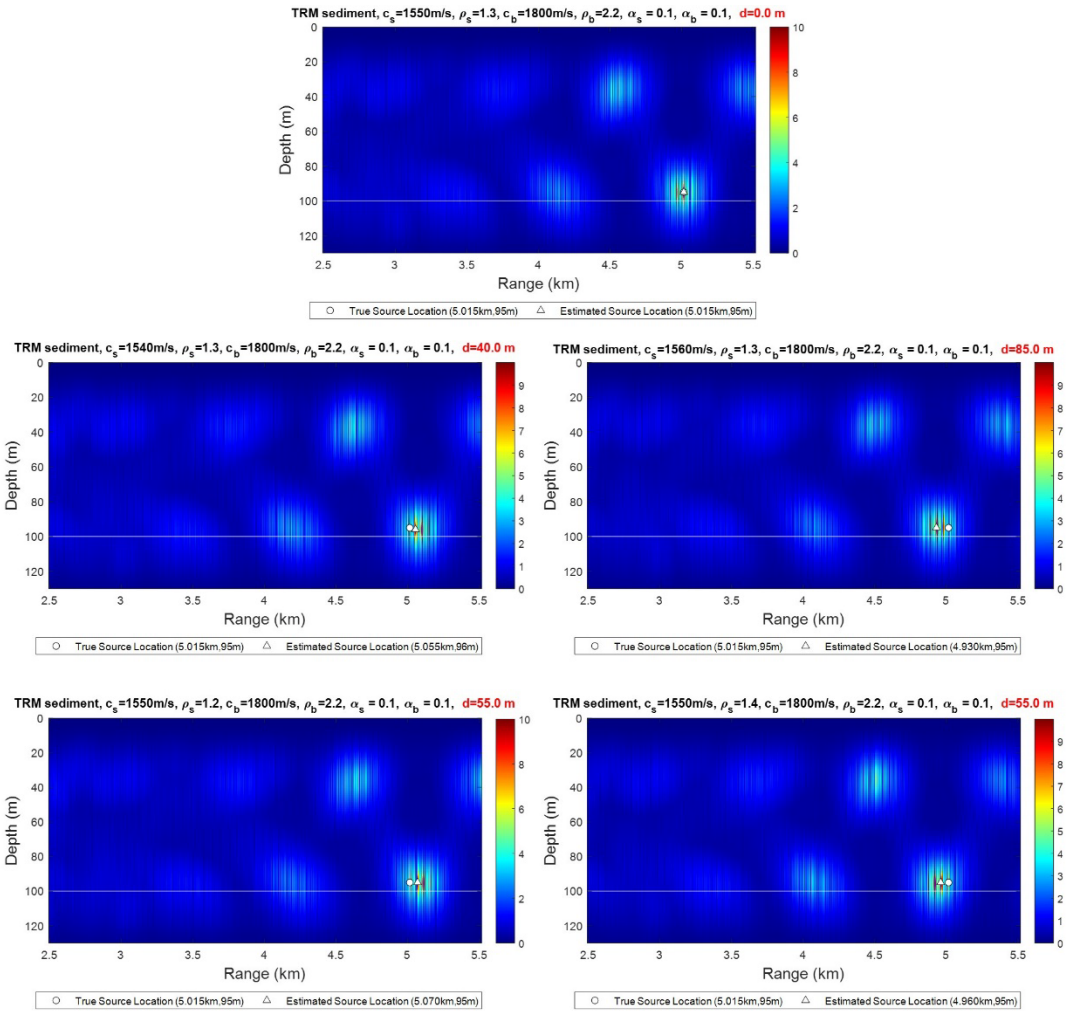

The sediment sound speed c_s and density ratio ρ_s are: (1st row-center) 1550 m/s and 1.3; (2nd row-left) 1540 m/s and 1.3; (2nd row-right) 1560 m/s and 1.3; (3rd row-left) 1550 m/s and 1.2; (3rd row-right) 1550 m/s and 1.4.

Figure 5. Reproduced effects of mismatched geoacoustic parameters on TRM focus

In our reproduction, the range dimension (along the x-axis) again referenced to the backward propagation. Thus, it appeared as a mirror image of the original. Otherwise, our reproduction accurately reflected the effects of mismatch geoacoustic parameters on the backward propagation and showed how the TRM focus was shifted. As documented by Godin et al. in [5], the TRM process is robust and focusing is possible with a single-element TRM. Additionally, position of the foci is more sensitive to sediment sound speed than sediment density.

3. Signals in the Time Domain

In the forward propagation, we plotted the source signal in the time domain arriving at the receiver, as a means to observe and compare the forward propagations in the various models studied in this research. Through inverse Fourier Transform, we converted the acoustical pressure from the frequency domain into the time domain, showing this in Figure 6 for the four homogeneous fluid bottom models and Figure 7 for the seabed with sediment layer model.

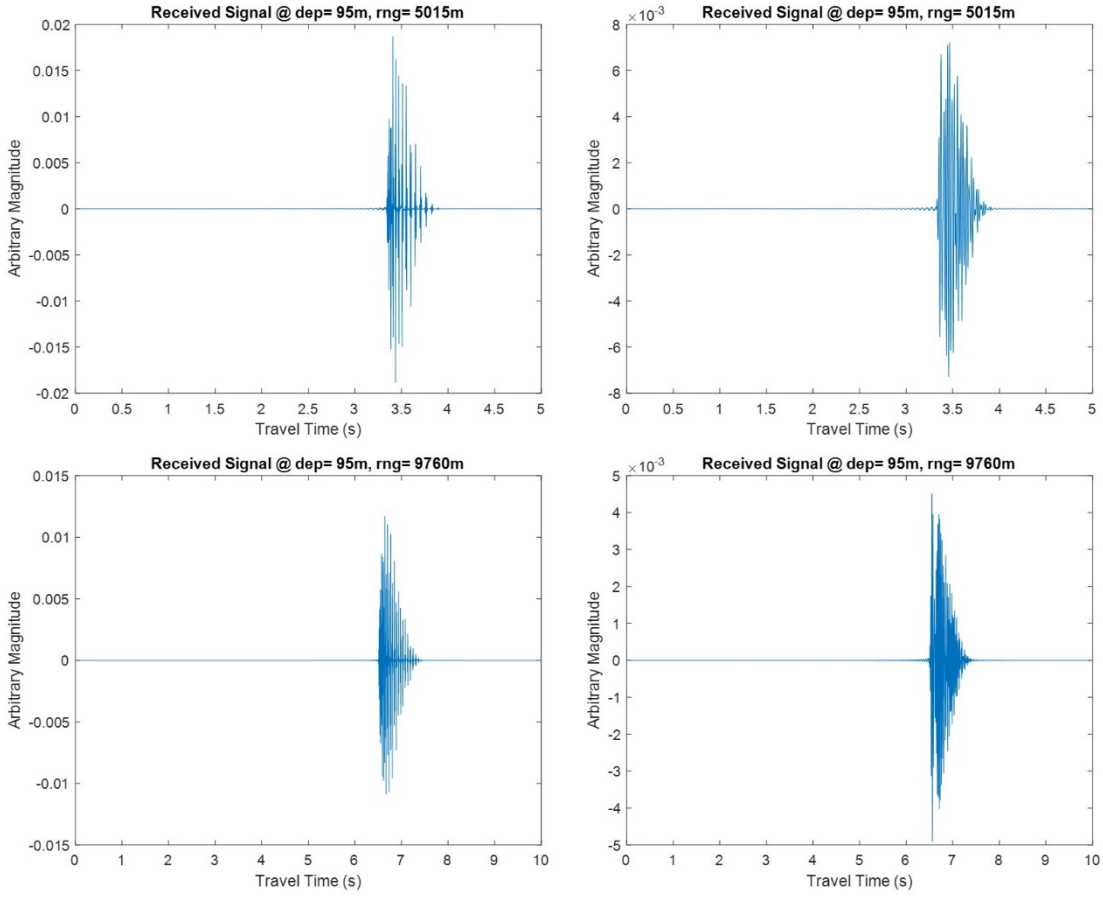

(Top-left) 5015 m range, 20–200Hz signal; (Top-right) 5015 m range, 20–70Hz signal; (Bottom-left) 9760 m range, 20–200Hz signal; (Bottom-right) 9760 m range, 20–200Hz signal.

Figure 6. Received signals for homogeneous fluid bottom models

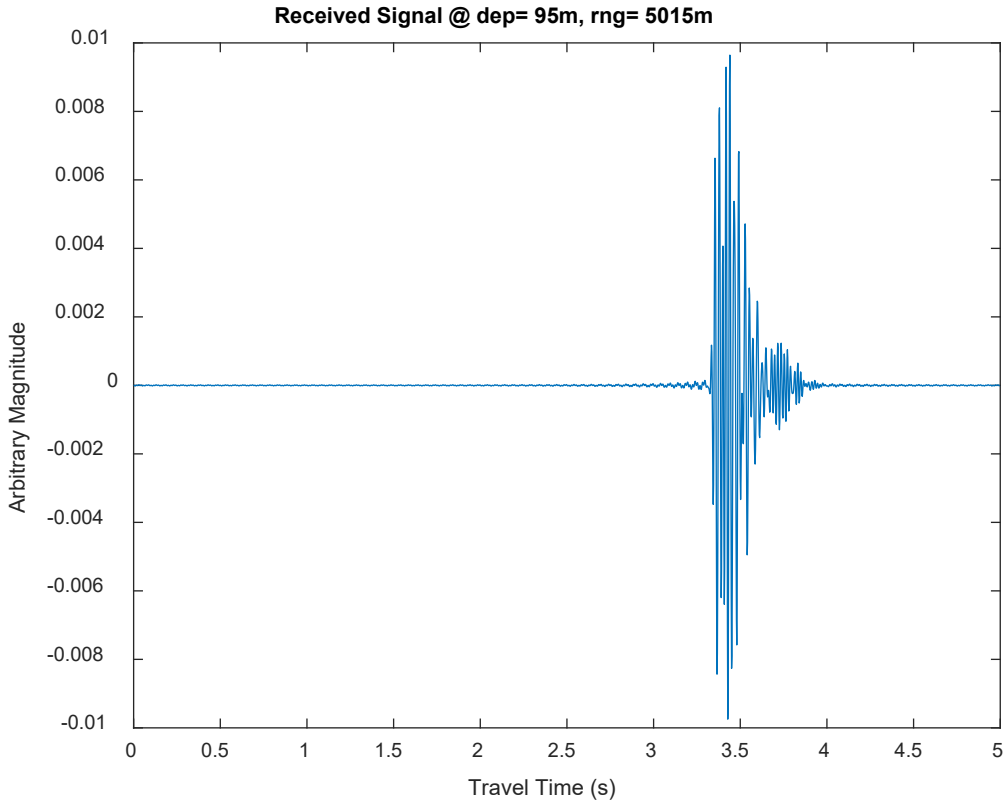

5015 m range, 20–70 Hz signal.

Figure 7. Received signal for seabed with sediment layer model

We observed that the causality of the received signal was reproduced accurately, which was unexpected from Fourier synthesis. There was a sharp response to the first arrival of the signal at the receiver, occurring at the expected time and producing a reasonable structure.

Subsequently, after computing the backward propagation and TRM foci, we took the respective acoustical pressures in the time domain and plotted the TRM signal. This was crucial as, subsequently, we established the use of the temporal focus as a metric for verifying the accuracy of our inverse problem solution. Figure 8 shows the TRM signal plotted in the time domain for the homogeneous fluid bottom models, and Figure 9 shows the TRM signals from the seabed with sediment layer model with different geoacoustic parameters used in the backward propagation.

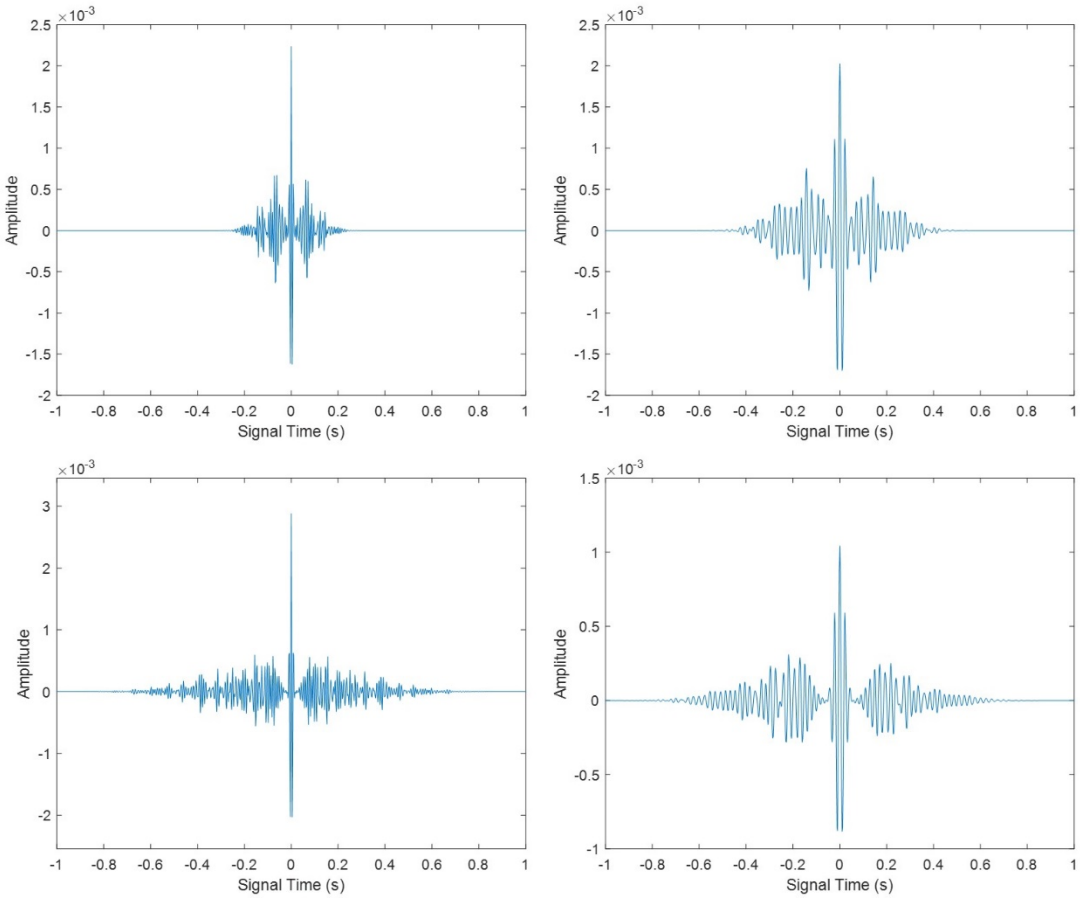

(Top-left) 5015 m range, 20–200Hz signal; (Top-right) 5015 m range, 20–70Hz signal; (Bottom-left) 9760 m range, 20–200Hz signal; (Bottom-right) 9760 m range, 20–200Hz signal.

Figure 8. TRM signals for homogeneous fluid bottom models

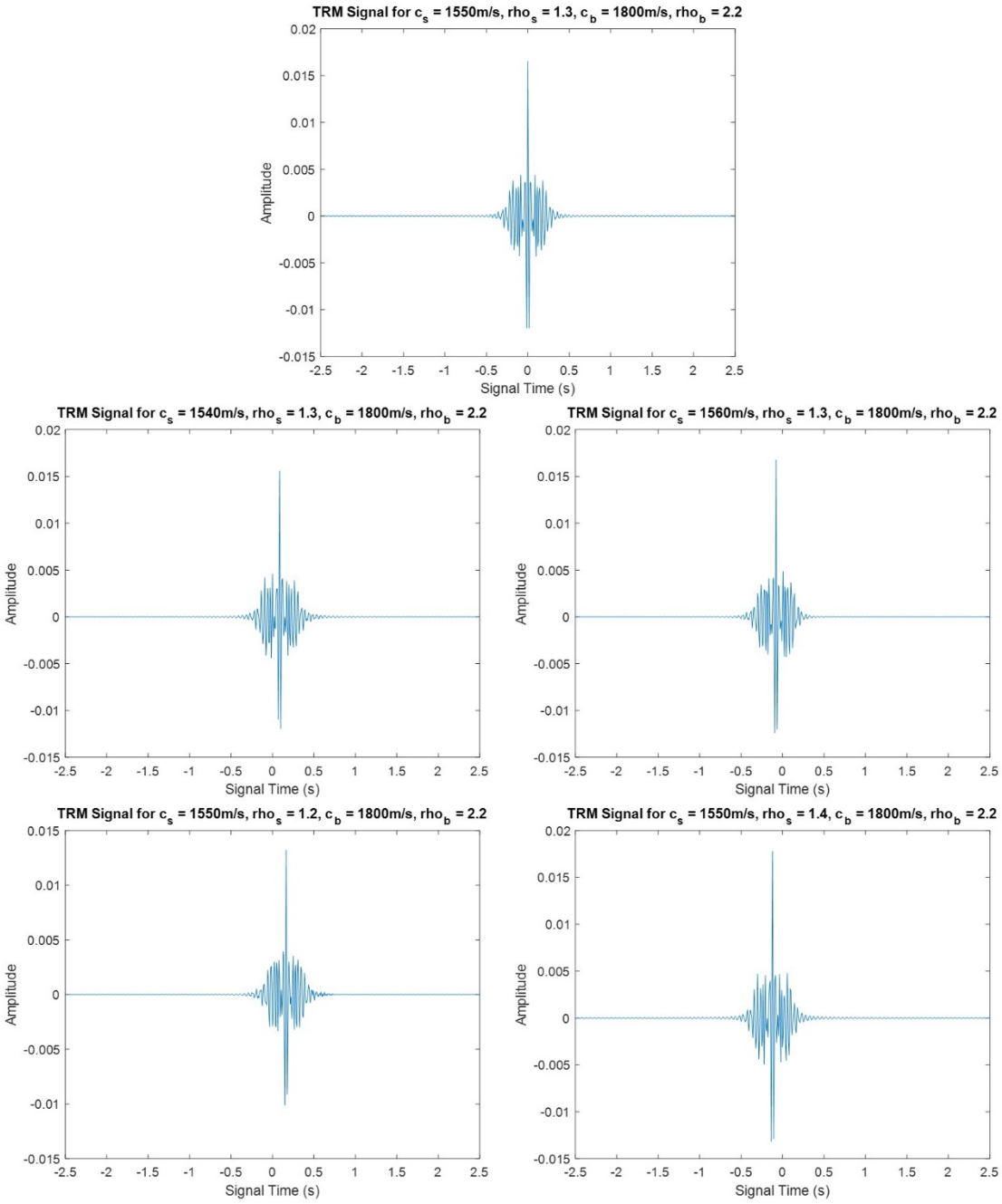

The sediment sound speed c_s and density ratio ρ_s are: (1st row-center) 1550 m/s and 1.3; (2nd row-left) 1540 m/s and 1.3; (2nd row-right) 1560 m/s and 1.3; (3rd row-left) 1550 m/s and 1.2; (3rd row-right) 1550 m/s and 1.4.

Figure 9. TRM signals for seabed with sediment layer model with mismatched geoacoustic parameters

Expectedly, the waveforms of the TRM signals differ significantly from the forward-propagated signals. They are compressed in time and symmetric as compared to the sharp onset observed in the forward-propagated signals. This is because the TRM signals represent the time-reversed focus, comprising the forward-received signals and the time-reversed signals [11].

By being able to successfully reproduce the single-element TRM in a homogeneous fluid bottom and replicate the effects of mismatched geoacoustic parameters, we were confident that our MATLAB RAM code was able to accurately model environments for our research.

D. AMBIGUOUS SOLUTIONS

Subsequent investigations revealed that while TRM was able to solve the inverse problem and obtain the unknown physical parameters of the ocean, a grid search invariably produced more than one possible combination of said unknown physical parameters. We concentrated on the two models that comprised a range of 5015 m between the source and receiver, with source signal bandwidths 20–200 Hz and 20–70 Hz, respectively, and conducted a grid search for parameters of bottom sound speed c_b and density ratio ρ_b.

To do this, we first numerically simulated the forward propagation, by setting c_b = 1750 m/s, density ratio ρ_b = 1.9, our true solution. Next, using ranges of values for each parameter, we calculated the backward propagation and applied TRM to arrive at the spatial focus. Table 5 shows the boundaries and steps of our grid search for the unknown parameters. We ensured that the true solution was one of the combinations of parameters for proper representation.

Table 5. Grid search settings for homogeneous fluid bottom models

	Range from	To	In steps of
Bottom sound speed, c_b (m/s)	1600	1800	10
Bottom density ratio, ρ_b	1.1	2.7	0.2
Total Number of Combinations	189		

For each combination, we zoomed in to the vicinity of the source's spatial position, as the high intensity associated with a TRM focus need not necessarily be the global maximum, but would categorically be a local maximum. These local maxima (for each combination of parameters) would be our respective TRM foci.

From there, we found the minimum range discrepancy (RD), defined as the horizontal distance between the TRM focus and the exact source position, and retrieved all the corresponding combinations. Table 6 presents the results.

Table 6. Ambiguous solutions from a grid search of the 5015 m homogeneous fluid bottom model

Source signal: 20–200 Hz
Minimum RD: 0.0 m
No. of combinations: 3

c_b (m/s)	ρ_b
1720	1.7
1750	1.9
1780	2.1

Source signal: 20–70 Hz
Minimum RD: 0.0 m
No. of combinations: 4

c_b (m/s)	ρ_b
1630	1.1
1710	1.5
1750	1.9
1780	2.3

We saw that geoacoustic parameters are interrelated and that their effects on the position of the TRM focus resulted in multiple possible combinations of parameters that still gave the minimum RD. Figure 10 graphically shows this ambiguity by plotting RD as a function of the two unknown parameters.

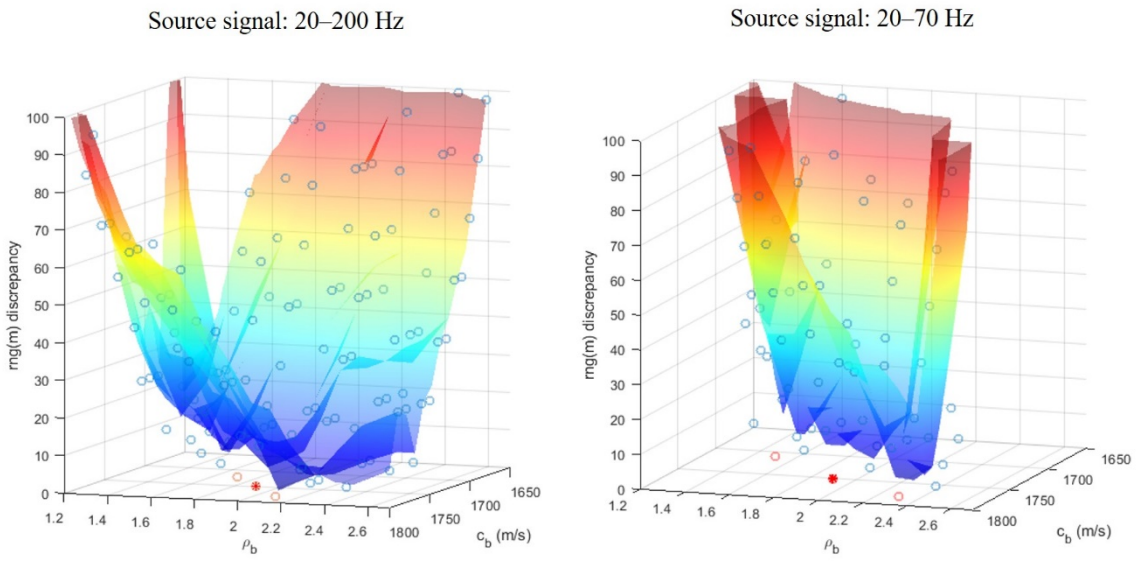

Blue circles represent combinations of unknown parameters; red circles represent combinations that result in a minimum RD; red asterisks signify the true solutions. (Left) 20–200 Hz signal; (Right) 20–70 Hz signal.

Figure 10. Ambiguous solutions in homogeneous fluid bottom models

The majority of the geoacoustic parameter combinations end up with large RD values, as evident in the many blue circles in the upper half of each plot (and many more beyond the visible axes of the plot). The colored gradient surface was added to provide a clearer representation of the valley produced by these combinations, culminating at the bottom with those that produced the minimum RD, as depicted by the red circles.

We observed that by filtering TRM foci based on RD, we arrived at ambiguous solutions. In the above two cases, there were multiple solutions that fit the criteria of minimum RD (0.0 m), and thus, the question was how to retrieve the true combination from among these ambiguous solutions.

THIS PAGE INTENTIONALLY LEFT BLANK

III. METHODOLOGY: METRICS

A. PARAMETERS FOR METRIC PRESENTATION

In this chapter, we describe the various metrics in consideration and detail how we expected them to sieve out the true combination from among the ambiguous solutions. We also anticipated being able to understand how the true solution and mismatched parameters would differ in their effects on the metrics. For illustrations, we used the homogeneous fluid bottom model from Chapter II, with parameters as shown in Table 7.

Table 7. Parameters of homogeneous fluid bottom models

Depth of water	100 m
Depth of source and receiver	95 m
Range from source to receiver	5015 m
Source signal bandwidth	20–200 Hz
Bottom sound speed, c_b	1750 m/s
Bottom density ratio, ρ_b (relative to the density of water)	1.9
Bottom attenuation, α_b (λ is the wavelength of sound)	0.3 dB/λ

To demonstrate suitability of the respective metrics, we first established how they work by calculating the back propagation and time-reversal mirror (TRM) process for two combinations of parameters, one that matched the forward propagation (c_b = 1650 m/s, ρ_b = 1.3) and the other with mismatched parameters (c_b = 1650 m/s, ρ_b = 1.3).

In the figures for this section, matched parameters are displayed on the left, and mismatched parameters are displayed on the right.

B. RANGE DISCREPANCY: MINIMUM

As detailed in the previous chapter, after solving the inverse problem using TRM, we established the first metric as minimum range discrepancy (RD) based on the position of the TRM focus. Figure 11 shows the example when the parameters matched the environmental conditions and when the parameters were mismatched.

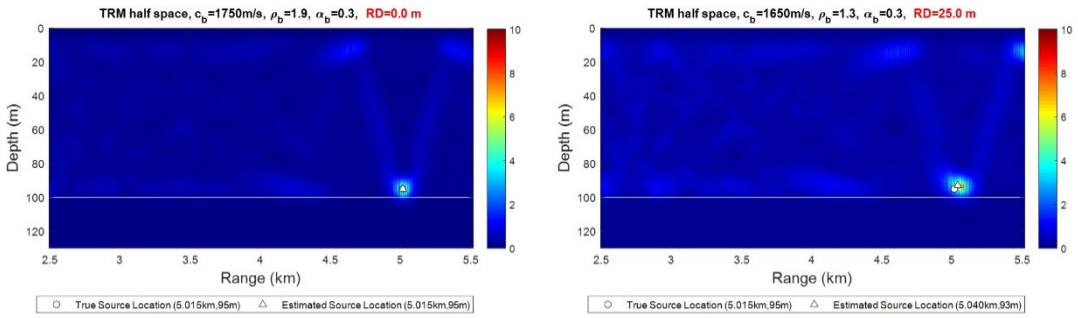

Figure 11. Spatial focus with matched and mismatched parameters

We soon realized that while useful in narrowing down the possibilities of suitable combinations, minimum RD alone was not sufficient to retrieve the true solution. While the above model and grid search resulted in two possible combinations, of which one is the true solution, given the relatively simple conditions, when numerical simulations increasingly reflect real world conditions, we expected the possibilities of suitable combinations to increase. Additionally, the choice of step size in the grid search also affects the number of ambiguous solutions obtained. This will be further discussed in Chapter IV. Thus, we would need more metrics to filter the mismatching parameters.

C. PEAK TIME: MINIMUM DEVIATION FROM ZERO

Returning to the theory of TRM, the process focuses the signal back both spatially and temporally [11]. With this, we hypothesized that another suitable metric, called peak time (PT), was determining that the signal was focused temporally, where in the time domain, it occurs closest to zero time [11]. To do this, we plotted the calculated TRM signals in the time domain and measured its proximity to zero time, the example shown in Figure 12. We observed that when mismatched parameters were used, the TRM signal did occur away from zero time.

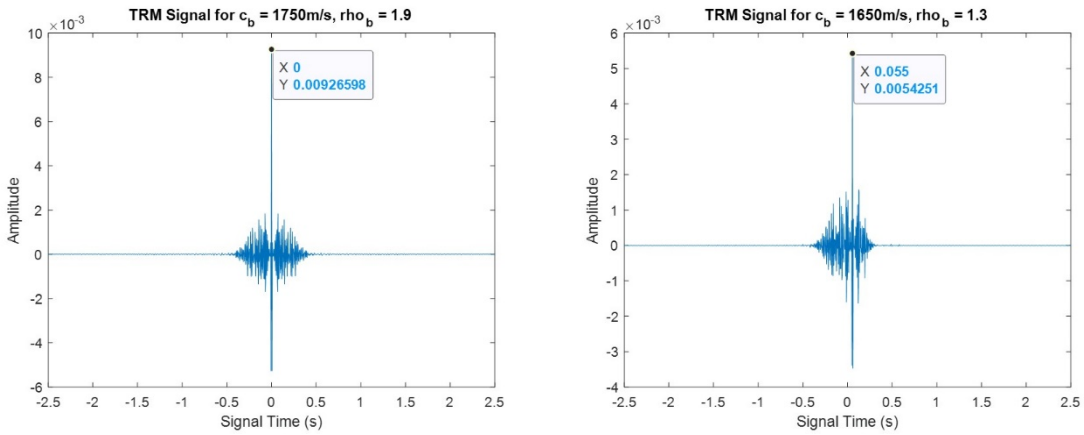

Figure 12. Temporal focus with matched and mismatched parameters

D. TIME WIDTH AT HALF HEIGHT: MINIMUM

Building on the concept of temporal focus, a proposed metric that exhibited potential was to measure the time width of the signal. We termed this metric time width at half height (TWHH). As the waveguide accommodates the various paths of the acoustic wave propagating through the environment, a compact TRM signal would mean higher likelihood of matching parameters as all the paths arrive closely. Conversely, a broad peak would mean that the energies of the signal were spread out over a longer time period.

We hypothesized that a suitable time width to measure should be interpolated between the time steps in our numerical simulation. Hence, we factored the height of the peak by half and noted the corresponding times to measure this width in time. Figure 13 demonstrates this for the example pair of parameter combinations, zooming in on the main peaks.

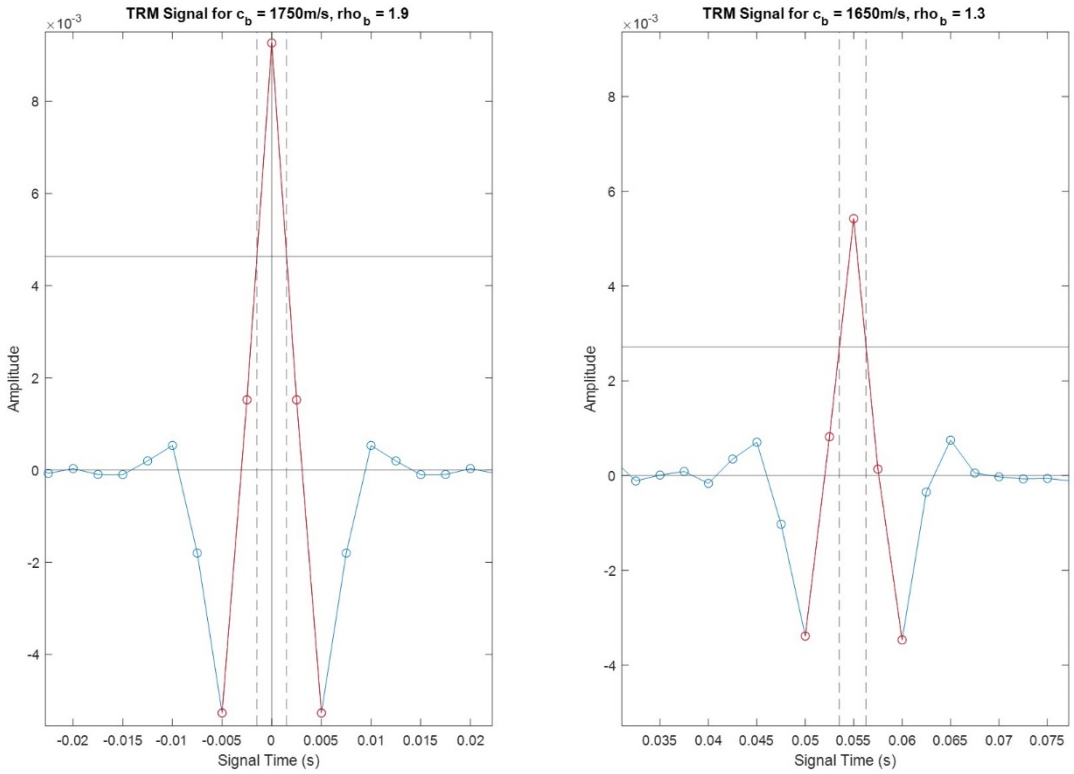

Figure 13. Time width of TRM signal at half peak height, matched and mismatched parameters

We plotted the TRM signal in blue, with data points represented by circles. The main peak was highlighted in red while the horizontal line (other than at zero amplitude) denoted half peak height. As previously described, the selection of time width was shown to be between data points.

The corresponding vertical dashed line represented the associated time value and this width formed the basis of this metric. Comparing the two combinations, with similar scales on the x-axis, the time width of true solution was narrower than with the mismatched parameters.

E. PEAK MAGNITUDE: MAXIMUM

For our plots in the time domain, peak magnitude (PM) represents the acoustical pressure at the TRM focus over time. Using an extension of the TWHH metric, we

hypothesized that only with the matched parameters will the peak be at a maximum due to the convergence of the different paths taken by the signal. When parameters are mismatched, the energy is spread out over time, lowering the magnitude of the peak. Referencing Figures 12 and 13, we observed the differences in the peaks when the matched and mismatched parameters were used.

F. SYMMETRY RATIO: MINIMUM

While studying the many plots of the TRM signals in the time domain, we made a visual observation that led to a possible new metric: when the parameters were matched, the TRM signal appeared symmetric about the main peak at zero time. We did not observe this symmetry when mismatched parameters were applied. Reference Figure 12 for depiction of this symmetry and its absence.

Anticipating that symmetry could be subjective and time consuming to identify among all the possible ambiguous solutions while solving an inverse problem, we attempted to find a way to be able to quickly and automatically analyze the TRM signals and compute a way of quantifying this symmetry. We proposed the following, comparing the odd and even functions of time. RHS and LHS refer to the right- and left-hand sides, respectively, of zero time.

$$\text{Symmetry Ratio (SR)} = \frac{\sum\left(RHS - LHS\right)^2}{\sum\left(RHS + LHS\right)^2}$$

This quantification resulted in a value that could be calculated rapidly and easily compared between TRM signals: the more symmetrical the peak, the smaller the value. For the examples referenced in this section, the two SR values were (1) 1.1700×10^{-32}, and (2) 0.6731, respectively. Visually, the plot on the left in Figure 10 shows symmetry as compared to the plot of the right (mismatched parameters). Our SR metric reflected this adequately. By our definition, it means that should the peak not be at zero time, the SR value will be significantly higher due to considerable asymmetry.

G. DEVELOPING THE SEQUENCE: RECIPE

We thus turned our attention towards developing a recipe, sequencing some or all of the metrics, to sieve through the various combinations efficiently and effectively, and arrive at the true solution.

IV. TEST AND EVALUATION

A. OVERVIEW

Using simulations of forward-propagated signals from various range-independent environmental models, we tested out the effectiveness of the individual metrics and applied them in a specific sequence to solve the inverse problem, through time-reversal mirror (TRM). We planned these increasingly realistic environmental models, each a step up from the previous, though not in chronological order of testing:

1. Homogeneous fluid bottom models, coarse grid search
2. Homogeneous fluid bottom models, fine grid search
3. Seabed with sediment layer models
4. Effects of noise (on models with sediment layer seabed)

In the grid search, our method of testing the metrics' suitability is by exploiting our knowledge of the true solution in our numerical simulations and ensuring that the true solution is one of the combinations tested. This allowed us to compare the metric values of ambiguous solutions and determine if the true solution has the best metric values. We list down the metrics and their criteria for reference in Table 8.

Table 8. Metrics and their criteria

Range Discrepancy (RD)	Minimum
Peak Time (PT)	Minimum deviation from zero
Symmetry Ratio (SR)	Minimum
Peak Magnitude (PM)	Maximum
Time Width of Half Height (TWHH)	Minimum

B. HOMOGENEOUS FLUID BOTTOM MODELS, COARSE GRID SEARCH

We first introduced the homogeneous fluid bottom models earlier in Chapter II, as both a reproduction of prior investigations as well as the introduction of the problem faced

that forms the basis of this thesis. Parameters of the homogeneous fluid bottom models are in Table 9, and the grid search settings are in Table 10.

Table 9. Parameters of homogeneous fluid bottom models

Depth of water	100 m
Depth of source and receiver	95 m
Range from source to receiver	5015 m
Source signal bandwidth	20–200 Hz
	20–70 Hz
Bottom sound speed, c_b	1750 m/s
Bottom density ratio, ρ_b (relative to the density of water)	1.9
Bottom attenuation, α_b (λ is the wavelength of sound)	0.3 dB/λ

Table 10. Coarse grid search settings for homogeneous fluid bottom models

	Range from	To	In steps of
Bottom sound speed, c_b (m/s)	1600	1800	10
Bottom density ratio, ρ_b	1.1	2.7	0.2
Total Number of Combinations	189		

Using the process of simulating the forward-propagating signal and processing it with TRM, Table 11 presents our metrics analysis, the true solutions highlighted in yellow.

Table 11. Metrics results for homogeneous fluid bottom models, coarse grid search

Combination	c_b	rho_b	RD	PT	SR	PM	TWHH
Source signal bandwidth 20–200 Hz							
A1	1720	1.7	0.0	0.0	0.013260	0.004086	0.002645
A2	1750	1.9	0.0	0.0	8.88×10^{-26}	0.004520	0.002646
A3	1780	2.1	0.0	0.0	0.012487279	0.004733	0.002703
Source signal bandwidth 20–70 Hz							
B1	1630	1.1	0.0	-0.002	0.514335	0.000775	0.007235
B2	1710	1.5	0.0	-0.002	0.483453	0.001536	0.007297
B3	1750	1.9	0.0	0.0	2.53×10^{-3}	0.002024	0.007291
B4	1780	2.3	0.0	0.002	0.393816	0.002279	0.007303

Combination A1 could be eliminated by PM, having the lowest value. Combination A3 could be eliminated by TWHH, having the highest value. Both would be eliminated by SR, with the true solution (A2) clearly identified. Combinations B1, B2, and B4 would be eliminated by PT. They would also be eliminated by SR, with the true solution, B3, clearly identified. We also observed that as per our definition of SR, when the TRM signal peak occurs away from zero time, the value of SR is substantially higher.

With the simplicity of this homogeneous fluid bottom environment and the relatively large step setting for the grid search, the ambiguous solutions were not very numerous. From the metrics and criteria set out in Chapter III, we found that in both cases, we were able to arrive at the true solution. Individually, the differences between PM and TWHH values appeared too close to be able to conclusively tell them apart. This is expected and hence the metrics are not expected to function alone but should be combined in a more sophisticated selection rule that we refer to as a recipe.

C. HOMOGENEOUS FLUID BOTTOM MODELS, FINE GRID SEARCH

Building on the previous case study, we use the same environmental model with parameters in Table 9 and apply a finer grid search with the settings shown in Table 12.

Table 12. Fine grid search settings for homogeneous fluid bottom models

	Range from	To	In steps of
Bottom sound speed, c_b (m/s)	1600	1800	5
Bottom density ratio, ρ_b	1.5	2.5	0.1
Total Number of Combinations	451		

Figure 14 graphically depicts the ambiguity of our solutions, and Table 13 then consolidates the results for this case study.

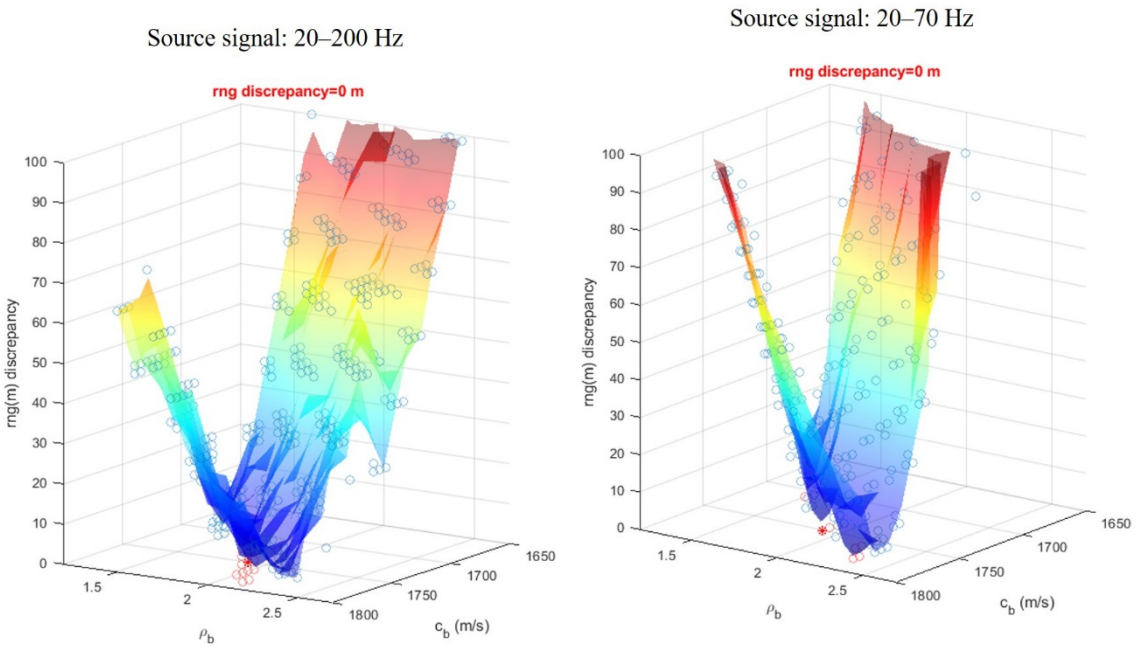

Blue circles represent combinations of mismatched parameters; red circles represent combinations that result in a minimum RD; red asterisks signify the true solution. (Left) 20–200 Hz signal; (Right) 20–70 Hz signal.

Figure 14. Ambiguous solutions in homogeneous fluid bottom models, fine grid search

Table 13. Metrics results for homogeneous fluid bottom models, fine grid search

Combination	c_b	rho_b	RD	PT	SR	PM	TWHH
Source signal bandwidth 20–200 Hz							
A1	1720	1.7	0.0	0.0	1.28×10^{-2}	0.004416	0.002510
A2	1730	1.8	0.0	0.0	0.004403	0.004613	0.002501
A3	1735	1.8	0.0	0.0	0.003066	0.004673	0.002509
A4	1740	1.8	0.0	0.0	0.013583	0.004692	0.002559
A5	1745	1.9	0.0	0.0	0.005272	0.004813	0.002534
A6	1750	1.9	0.0	0.0	1.58×10^{-32}	0.004872	0.002518
A7	1755	1.9	0.0	0.0	5.11×10^{-3}	0.004893	0.002538
A8	1760	2.0	0.0	0.0	0.012042	0.004952	0.002578
A9	1765	2.0	0.0	0.0	0.002985	0.005011	0.002538
A10	1770	2.0	0.0	0.0	0.002995	0.005037	0.002531
A11	1775	2.0	0.0	0.0	0.011497	0.005029	0.002555
A12	1780	2.1	0.0	0.0	0.012094	0.005096	0.002573
A13	1785	2.1	0.0	0.0	0.007146	0.005128	0.002541

Combination	c_b	rho_b	RD	PT	SR	PM	TWHH
Source signal bandwidth 20–70 Hz							
B1	1710	1.5	0.0	-0.002	0.463423	0.000724	0.006761
B2	1745	1.9	0.0	0.0	0.007878	0.000932	0.006827
B3	1750	1.9	0.0	0.0	0.001710	0.000947	0.006798
B4	1760	2.2	0.0	0.002	0.496349	0.001011	0.006814
B5	1765	2.2	0.0	0.002	0.360956	0.001023	0.006821
B6	1775	2.3	0.0	0.002	0.536868	0.001051	0.006833
B7	1780	2.3	0.0	0.002	0.402528	0.001061	0.006761

In this case study, the finer-grid search produced a significantly higher number of possible combinations from minimum RD. In combination set A, all possibilities had PT at zero time, and SR clearly indicated the true solution. We noted, however, that the true solution did not exhibit the highest PM or the smallest TWHH.

For combination set B, PT quickly narrowed down the list to two and showed the true solution with the higher PM and smaller TWHH, albeit by only a small margin. While the difference in SR was not as striking, the true solution was about 4.5 times smaller than the other possible combination and could still be considered sufficiently significant to identify the true solution. Delving further into this, Figure 15 plots these two TRM signals in the time domain, for a visual analysis.

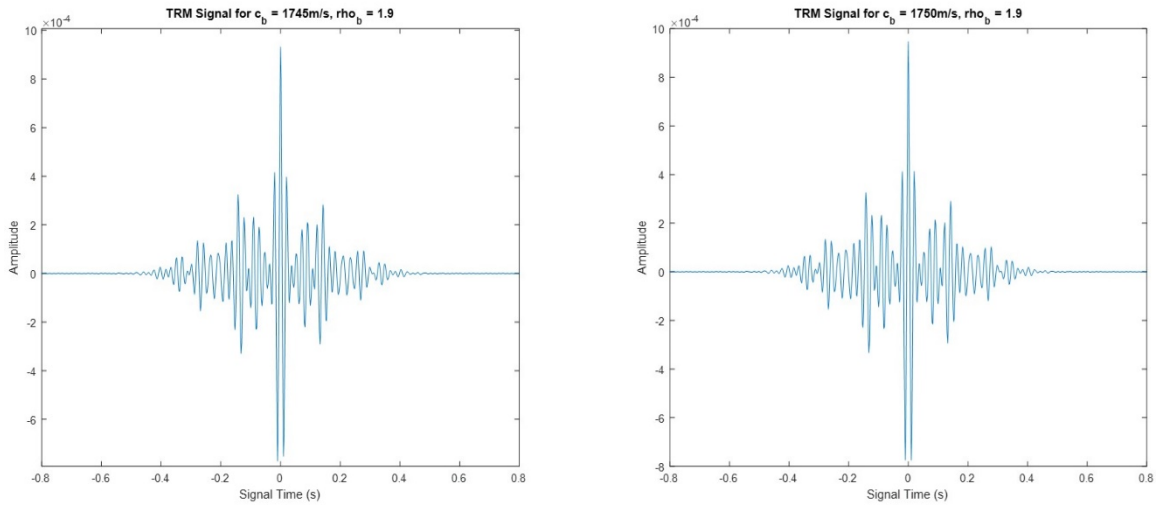

Figure 15. Visual analysis of TRM signals for combinations B2 and B3

Upon visual inspection, specifically looking at the two minima and two adjacent peaks on either side of the main peak, the plot on the left (with mismatched parameters) demonstrates slight asymmetry while the plot with the true solution (right) appears quite symmetrical, and this concurred with the conclusion drawn from the SR values.

With these observations, we inferred that the metrics used in the particular sequence of RD, PT, and SR works reasonably well to sieve out the true solution.

D. SEABED WITH SEDIMENT LAYER MODELS

Increasing the complexity and realism, we added a sediment layer into our environmental model. The parameters are shown in Table 14. Stepping up from the homogeneous fluid bottom models with two unknown parameters, our sediment layer models have five unknown parameters, which are reflected in the grid search settings in Table 15.

Table 14. Parameters of seabed with sediment layer models

Depth of water	100 m
Depth of source and receiver	95 m
Range from source to receiver	5015 m
Source signal bandwidth	20–200 Hz
	20–70 Hz
Sediment thickness, H	20 m
Sediment sound speed, c_b	1550 m/s
Sediment density ratio, ρ_b (relative to the density of water)	1.3
Sediment attenuation, α_b (λ is the wavelength of sound)	0.1 dB/λ
Bottom sound speed, c_b	1800 m/s
Bottom density ratio, ρ_b (relative to the density of water)	2.2
Bottom attenuation, α_b (λ is the wavelength of sound)	0.1 dB/λ

Table 15. Grid search settings for seabed with sediment layer models

	Range from	To	In steps of
Sediment thickness, H (m)	10	30	10
Sediment sound speed, c_s (m/s)	1510	1590	20
Sediment density ratio, ρ_s	1.0	1.9	0.3
Bottom sound speed, c_b (m/s)	1740	1830	30
Bottom density ratio, ρ_b	1.9	2.5	0.3
Total Number of Combinations	720		

With five independent variables in our unknown parameters, it was no longer feasible to present graphically our dependent variable, RD, as a function of the independent variables. The grid search, however, systematically tested out every combination of unknown parameters. Applying the first metric of RD, the list of possible combinations are presented in Table 16.

Table 16. Metrics results for seabed with sediment layer models

Combination	H	c_s	rho_s	c_b	rho_b	RD	PT	SR	PM	TWHH
Source signal bandwidth 20–200 Hz										
A1	10	1530	1.0	1830	2.2	0.0	0.0	0.182749	0.002384	0.002769
A2	20	1550	1.3	1770	1.9	0.0	0.0	0.011686	0.003021	0.002817
A3	20	1550	1.3	1800	2.2	0.0	0.0	8.54×10^{-26}	0.003122	0.002840
A4	20	1550	1.3	1830	2.5	0.0	0.0	0.009208	0.003067	0.002833
A5	30	1550	1.3	1830	1.9	0.0	0.0	0.107060	0.002467	0.002725
Source signal bandwidth 20–70 Hz										
B1	20	1550	1.3	1740	1.9	0.0	0.0	0.011993	0.000749	0.007020
B2	20	1550	1.3	1800	2.2	0.0	0.0	9.55×10^{-25}	0.000800	0.006951
B3	30	1530	1.3	1770	1.9	0.0	0.0	0.282985	0.000449	0.041997
B4	30	1550	1.9	1830	1.9	0.0	0.004	4.819642	0.000814	0.008005

We initially expected that the introduced complexity and realism from the seabed with sediment layer would pose challenges for our metrics. The results showed that in both models, however, the true solution was still identified with a high degree of confidence. The following observations were made:

1. There was one mismatched combination that peak time was not at zero time for source signal 20–70 Hz.
2. In both cases, SR confidently identified the true solution.
3. In both cases, the true solution had the highest PM.
4. In both cases, the true solution did not have the smallest TWHH.

E. EFFECTS OF NOISE

With increased confidence in our recipe, we next moved to introduce random noise into our signal. Stochastic noise is omnipresent in the real world, from manmade sources such as shipping, to marine life and biologics, even natural phenomena such as precipitation and bubbles; these all produce sound and could potential affect our TRM process with their varied intensities.

Our method of evaluation was to insert in the forward-propagating signal, white Gaussian noise with decreasing signal-to-noise ratios (SNR) in order to simulate a realistic environment, while evaluating the robustness of our metrics to cope. In our code, our simulated signal was measured for its power and thereafter noise corresponding to the respective SNR was added.

Our random white noise was added in the following sequence:

1. SNR = 40 dB
2. SNR = 20 dB
3. SNR = 10 dB
4. SNR = 5 dB
5. SNR = 0 dB

Noise was added in the forward propagation to our simulated signal as it reached our TRM. We anticipated that white noise corresponding to SNR = 40 dB would have minimal effects as compared to the noiseless environment, but it would provide the baseline for comparison of the models in this section.

The models in this section have similar parameters as those without noise added. Table 17 recaps these parameters, and Table 18 shows the enacted grid search settings.

Table 17. Parameters of seabed with sediment layer models

Depth of water	100 m
Depth of source and receiver	95 m
Range from source to receiver	5015 m
Source signal bandwidth	20–200 Hz
	20–70 Hz
Sediment thickness, H	20 m
Sediment sound speed, c_b	1550 m/s
Sediment density ratio, ρ_b (relative to the density of water)	1.3
Sediment attenuation, α_b (λ is the wavelength of sound)	0.1 dB/λ
Bottom sound speed, c_b	1800 m/s
Bottom density ratio, ρ_b (relative to the density of water)	2.2
Bottom attenuation, α_b (λ is the wavelength of sound)	0.1 dB/λ

Table 18. Grid search settings for seabed with sediment layer models

	Range from	To	In steps of
Sediment thickness, H (m)	10	30	10
Sediment sound speed, c_s (m/s)	1510	1590	20
Sediment density ratio, ρ_s	1.0	1.9	0.3
Bottom sound speed, c_b (m/s)	1740	1830	30
Bottom density ratio, ρ_b	1.9	2.5	0.3
Total Number of Combinations	720		

First, we demonstrated the effects of noise on the received signals. In Figure 16, we plotted the received signals, with source bandwidth 20–70 Hz, in the forward propagation. For comparison, we also included the signal with no added noise. As predicted, the plots of the noise-less signal and the model with noise corresponding to SNR = 40 dB were

almost identical. As SNR decreased, the presence of noise became increasingly apparent in the plots of received signal.

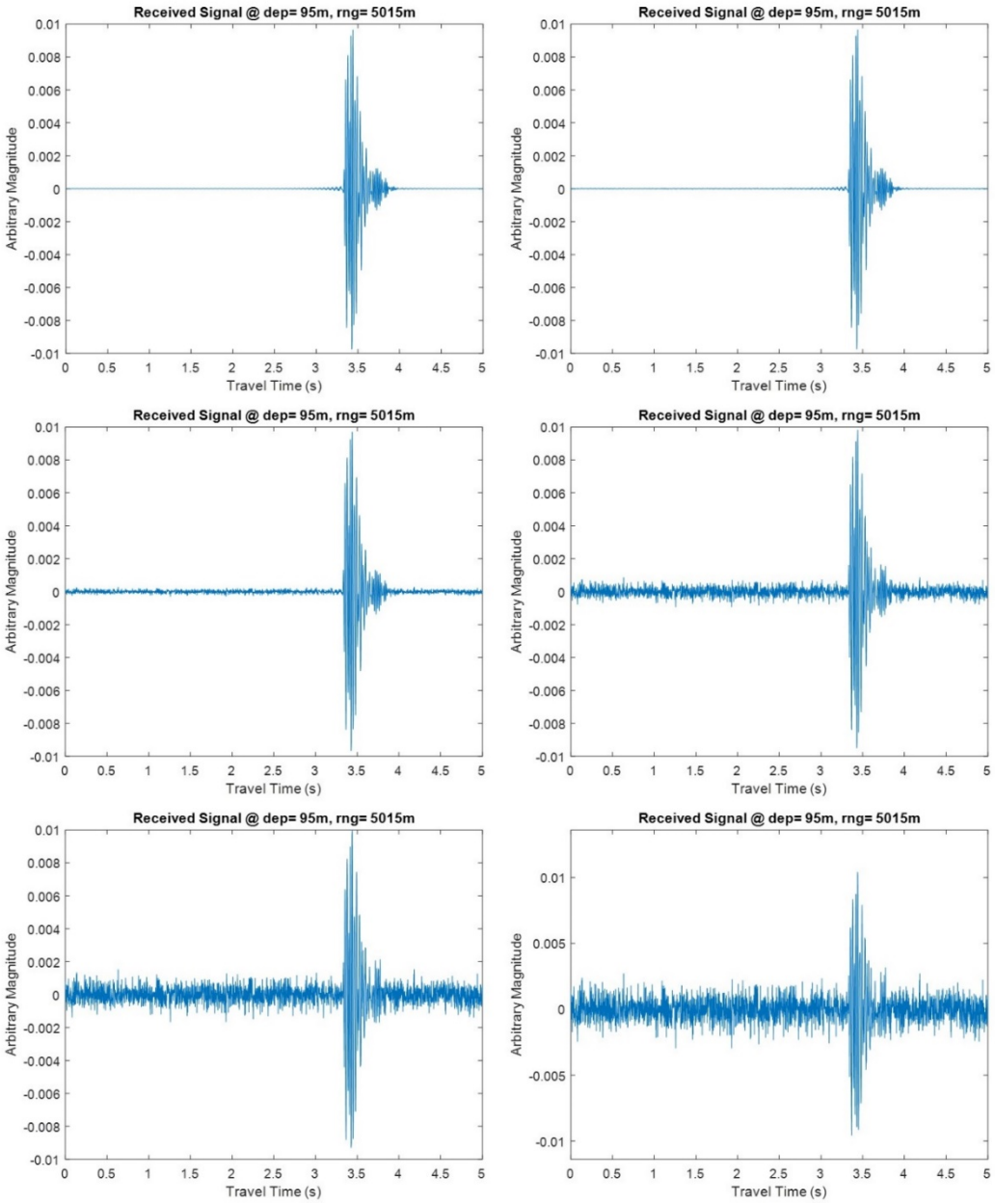

(1st row-left) With no added noise; (1st row-right) With noise of SNR = 40 dB; (2nd row-left) With noise of SNR = 20 dB; (2nd row-right) With noise of SNR = 10 dB; (3rd row-left) With noise of SNR = 5 dB; (3rd row-right) With noise of SNR = 0 dB.

Figure 16. Received signals with noise of increasing SNR, signal bandwidth 20–70 Hz

As a check, we subtracted the received signal without noise from the signal with noise corresponding to SNR = 40 dB added. Figure 17 shows the realization of the added random noise.

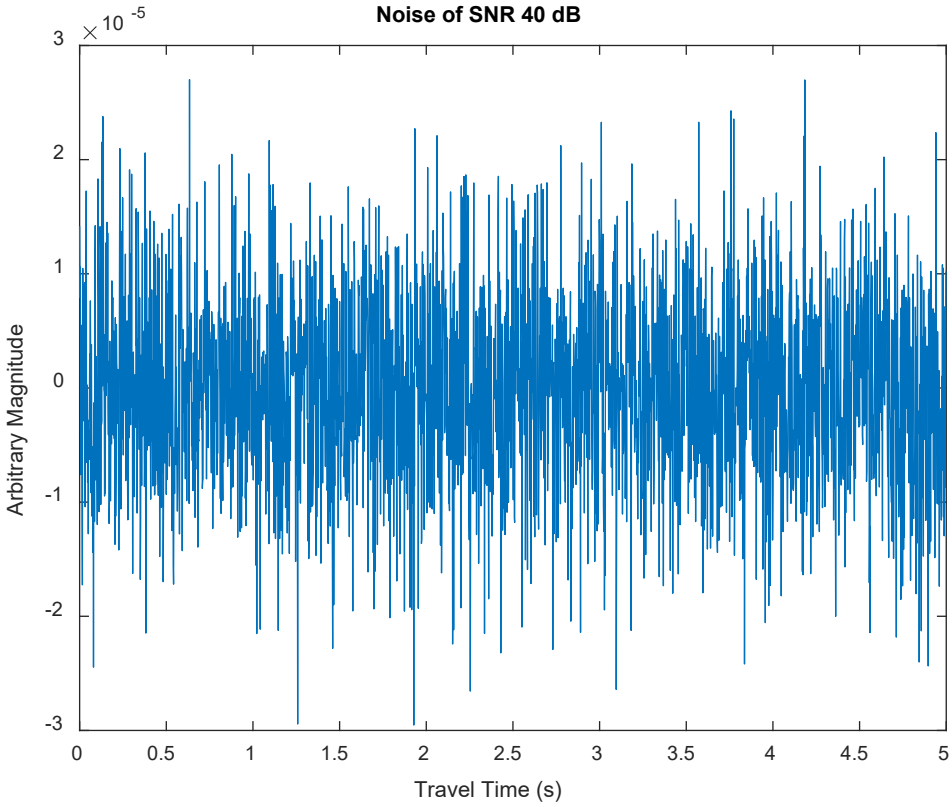

Figure 17. Verification of noise added, difference between signals with and without noise

We were now confident of simulating environments with white Gaussian noise and were ready to proceed with analyzing our metrics' performance.

1. SNR = 40 dB

Organized in Table 19 are the metrics results from the seabed with sediment layer models with added noise corresponding to SNR = 40 db.

Table 19. Metrics results for seabed with sediment layer models with added noise, SNR = 40 dB

Combination	H	c_s	rho_s	c_b	rho_b	RD	PT	SR	PM	TWHH
Source signal bandwidth 20–200 Hz										
A1	10	1530	1.0	1830	2.2	0.0	0.0	0.183065	0.002384	0.002770
A2	20	1550	1.3	1770	1.9	0.0	0.0	0.011657	0.003022	0.002817
A3	20	1550	1.3	1800	2.2	0.0	0.0	6.84×10^{-6}	0.003123	0.002840
A4	20	1550	1.3	1830	2.5	0.0	0.0	0.009245	0.003067	0.002834
A5	30	1550	1.3	1830	1.9	0.0	0.0	0.107179	0.002468	0.002725
Source signal bandwidth 20–70 Hz										
B1	20	1550	1.3	1740	1.9	0.0	0.0	0.004855	0.002455	0.007621
B2	20	1550	1.3	1800	2.2	0.0	0.0	2.22×10^{-6}	0.002557	0.007605

As all combinations had PT at zero time, this metric was unable to narrow the possibilities. By the time we used the metric SR, we were able to identify the matched combination with a high degree of confidence. The difference between SR values from matched and mismatched combinations was less apparent (four orders of magnitude, compared to 25 orders of magnitude in the noiseless environment) and this was expected as the random noise in the received signal would reduce the symmetry of the TRM signals.

Other observations are as follows:

1. PM for the true solution was the highest among the combinations.
2. TWHH was not the lowest for the test involving the 20–200 Hz source signal; the lowest was in combination set B (20–70 Hz), which had two possibilities.

2. SNR = 20 dB

Next, we increased the noise in the environment, such that the signal received contained noise corresponding to SNR = 20 dB. Table 20 displays the metrics results.

Table 20. Metrics results for seabed with sediment layer models with added noise, SNR = 20 dB

Combination	H	c_s	rho_s	c_b	rho_b	RD	PT	SR	PM	TWHH
Source signal bandwidth 20–200 Hz										
A1	10	1530	1.0	1830	2.2	0.0	0.0	0.186712	0.002383	0.002775
A2	20	1550	1.3	1770	1.9	0.0	0.0	0.012051	0.003027	0.002822
A3	20	1550	1.3	1800	2.2	0.0	0.0	0.0006811	0.003127	0.002845
A4	20	1550	1.3	1830	2.5	0.0	0.0	0.010201	0.003069	0.002838
A5	30	1550	1.3	1830	1.9	0.0	0.0	0.108947	0.002468	0.002731
Source signal bandwidth 20–70 Hz										
B1	20	1550	1.3	1740	1.9	0.0	0.0	0.004992	0.002459	0.007621
B2	20	1550	1.3	1800	2.2	0.0	0.0	0.0002211	0.002562	0.007603

In what continued to be a trend as we increased the random noise in the environment and the signal, we again see that while SR was able to identify conclusively the true solution, the difference between values from matched and unmatched parameters was now one order of magnitude. This was as compared to four orders of magnitude in the case of added noise corresponding to SNR = 40 dB.

Other observations are as follows:

1. PM for the true solution was the highest among the combinations.
2. TWHH was not the lowest for the test involving the 20–200 Hz source signal; the lowest was in combination set B (20–70 Hz), which had two possibilities.

These observations were similar to the tests with the seabed with sediment layer models, in both environments without noise and with noise corresponding to SNR = 40 dB, and we noted the trend regarding the effectiveness of PM and TWHH.

3. SNR = 10 dB

The next model analyzed had noise added corresponding to SNR = 10 dB. Displayed in Table 21 are the metrics results of this test.

Table 21. Metrics results for seabed with sediment layer models with added noise, SNR = 10 dB

Combination	H	c_s	rho_s	c_b	rho_b	RD	PT	SR	PM	TWHH
Source signal bandwidth 20–200 Hz										
A1	10	1510	1.9	1800	2.5	0.0	0.004	1.202084	0.002476	0.007600
A2	10	1530	1.0	1830	2.2	0.0	0.0	0.201235	0.002382	0.002786
A3	20	1550	1.3	1770	1.9	0.0	0.0	0.017673	0.003038	0.002833
A4	20	1550	1.3	1800	2.2	0.0	0.0	0.006701	0.003137	0.002857
A5	20	1550	1.3	1830	2.5	0.0	0.0	0.017057	0.003075	0.002849
A6	30	1550	1.3	1830	1.9	0.0	0.0	0.118173	0.002468	0.007600
Source signal bandwidth 20–70 Hz										
B1	20	1550	1.3	1740	1.9	0.0	0.0	0.006773	0.002469	0.007618
B2	20	1550	1.3	1800	2.2	0.0	0.0	0.002193	0.002573	0.007598
B3	30	1550	1.9	1830	1.9	0.0	0.004	4.827056	0.002678	0.008586

In these models, our SR metric faced even greater obstacles in identifying the true solution. The difference between values from matched and unmatched parameters was now only a factor of 2.5 in set A combinations, and three in set B combinations. While still possibly sufficient to identify the true solution with confidence, the decrease in difference as SNR increased was a trend to take note of.

For reference, we plotted the TRM signals for combinations A4, A5, B1, and B2 in Figure 18.

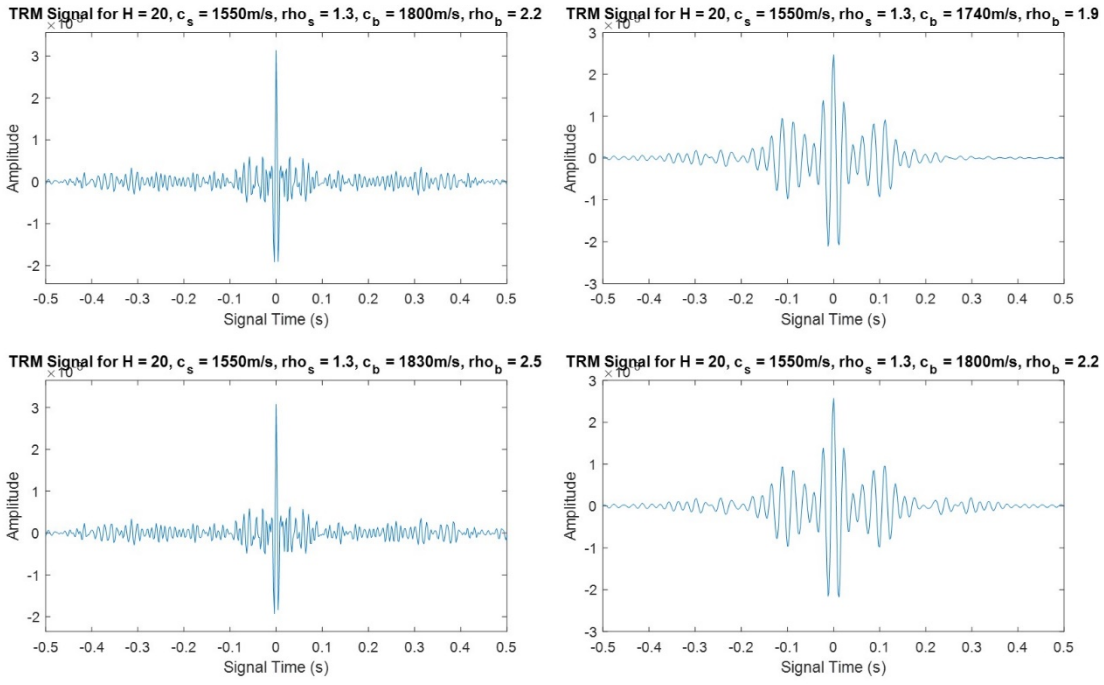

(Left) TRM signals of combination A4 (top) and A5 (bottom); (Right) TRM signals of combination B1 (top) and B2 (bottom)

Figure 18. TRM signals, combinations A4 and A5, B1 and B2

We verified visually and observed that in the left plots of A4 and A5, asymmetry was slight but present in A5 (bottom) by focusing on the two minima on either side of the main peak. Similarly, in the right pair of B1 and B2, the asymmetry in B1 (top) is

observable in the two minima and two adjacent secondary peaks on either side of the main peak.

Other observations are as follows:

1. PM for the true solution was the highest among the combinations.
2. TWHH was not the lowest for the test involving the 20–200 Hz source signal; the lowest was in combination set B (20–70 Hz), which had two possibilities.

4. SNR = 5 dB

In our penultimate test for the environments with noise added, we analyzed the signal with noise corresponding to SNR = 5 dB added. Table 22 documents our results.

Table 22. Metrics results for seabed with sediment layer models with added noise, SNR = 5 dB

Combination	H	c_s	rho_s	c_b	rho_b	RD	PT	SR	PM	TWHH
Source signal bandwidth 20–200 Hz										
A1	10	1510	1.9	1800	2.5	0.0	0.004	1.185846	0.002505	0.007616
A2	20	1550	1.3	1770	1.9	0.0	0.0	0.031608	0.003051	0.002845
A3	20	1550	1.3	1800	2.2	0.0	0.0	0.020651	0.003149	0.002870
A4	20	1550	1.3	1830	2.5	0.0	0.0	0.032194	0.003081	0.002861
A5	30	1550	1.3	1830	1.9	0.0	0.0	0.136687	0.002469	0.002762
Source signal bandwidth 20–70 Hz										
B1	20	1550	1.3	1740	1.9	0.0	0.0	0.011231	0.002479	0.007616
B2	20	1550	1.3	1800	2.2	0.0	0.0	0.006853	0.002585	0.007592

SR was still able to identify the true solution as they were the combinations with the lowest values. The difference between the SR values of matched and mismatched parameters was now a factor of 1.5. We thus expected to have difficulties differentiating symmetry and asymmetry from the plots.

Figure 19 shows the TRM signals comparing combinations A2 and A3 (the two combinations in set A with the closest SR), and combinations B1 and B2.

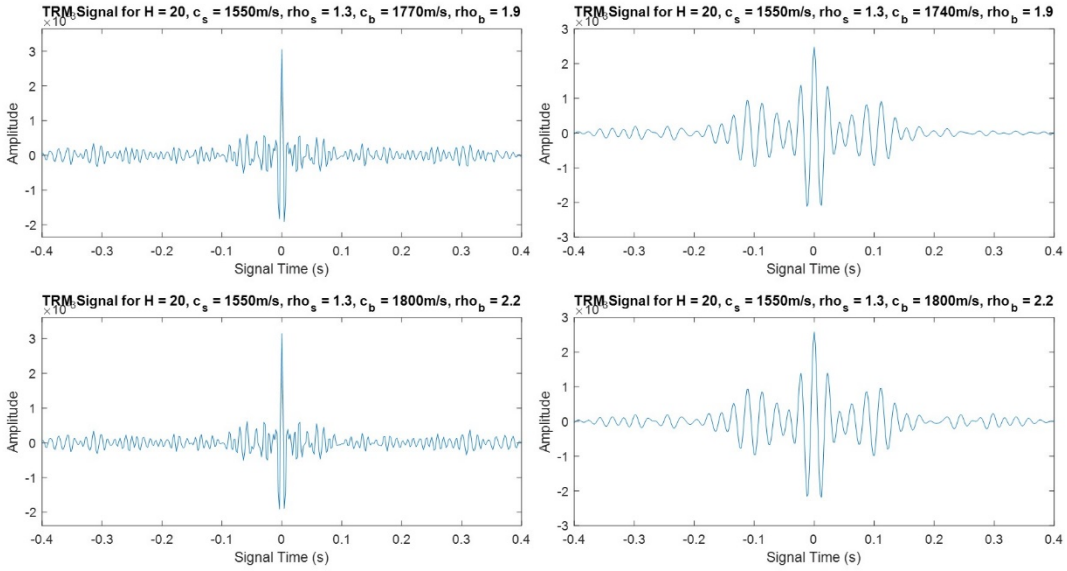

(Left) TRM signals of combination A2 (top) and A3 (bottom); (Right) TRM signals of combination B1 (top) and B2 (bottom)

Figure 19. TRM signals, combinations A2 and A3, B1 and B2

Visually, slight asymmetry is observed in A2, in the left pair, between the two minima on either side of the main peak. On the right pair, TRM signals from B1 and B2 appear equally symmetrical. Noise corresponding to SNR = 5 dB seemed to be the cutoff where visual assessment was no longer reliable.

Other observations are as follows:

1. PM for the true solution was the highest among the combinations.

2. TWHH was not the lowest for the test involving the 20–200 Hz source signal; the lowest was in the two-possibility combination set B (20–70 Hz).

3. After classification by SR, PM can be used to reinforce identification of the true solution.

5. SNR = 0 dB

For completeness, the signal was simulated with noise corresponding to SNR = 0 dB and the metrics were put through their paces to assess their effectiveness. Table 23 documents the results.

Table 23. Metrics results for seabed with sediment layer models with added noise, SNR = 0 dB

Combination	H	c_s	rho_s	c_b	rho_b	RD	PT	SR	PM	TWHH
Source signal bandwidth 20–200 Hz										
A1	10	1510	1.9	1800	2.5	0.0	0.004	1.144261	0.002556	0.007644
A2	20	1550	1.3	1770	1.9	0.0	0.0	0.073189	0.003073	0.002868
A3	20	1550	1.3	1800	2.2	0.0	0.0	0.061317	0.003170	0.002894
A4	20	1550	1.3	1830	2.5	0.0	0.0	0.075496	0.003093	0.002883
Source signal bandwidth 20–70 Hz										
B1	20	1550	1.3	1740	1.9	0.0	0.0	0.025154	0.002499	0.007612
B2	20	1550	1.3	1800	2.2	0.0	0.0	0.021061	0.002607	0.007582

As expected, while the true solution still exhibited the lowest SR value, the difference between SR values for matched and mismatched parameters was even closer. The random nature of the added noise had made the TRM signal with matched parameters equally asymmetrical as the signal with mismatched parameters.

Figure 20 shows the TRM signals comparing combinations A2 and A3 (the two combinations in set A with the closest SR) and combinations B1 and B2.

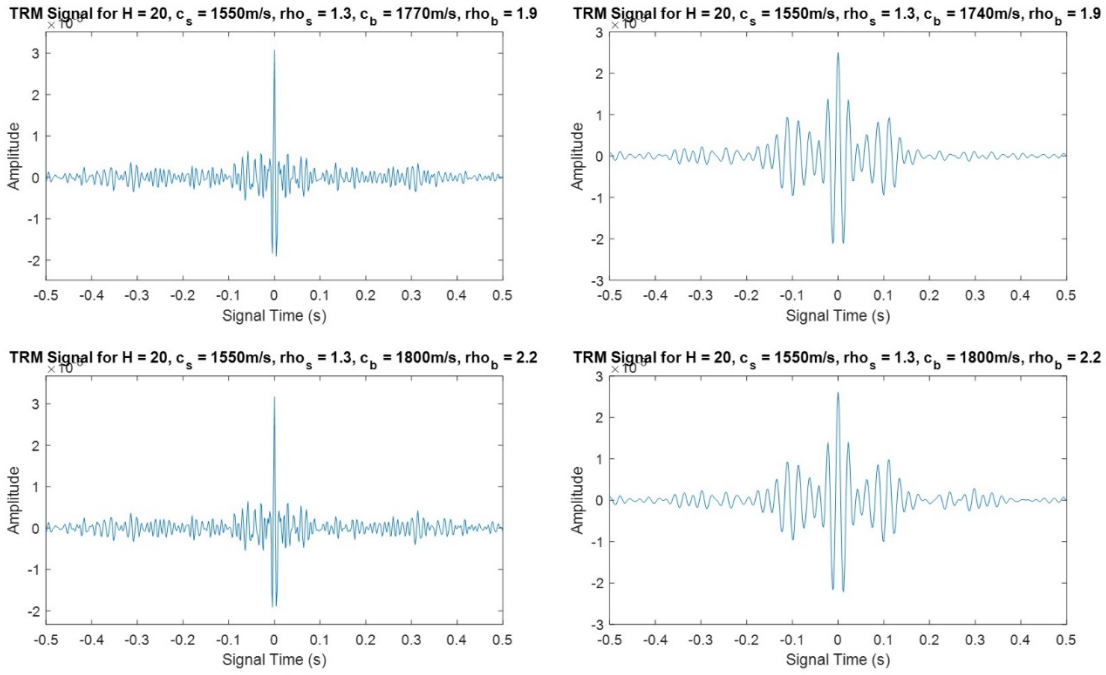

(Left) TRM signals of combination A2 (top) and A3 (bottom); (Right) TRM signals of combination B1 (top) and B2 (bottom)

Figure 20. TRM signals, combinations A2 and A3, B1 and B2

As anticipated from the trending thus far (of the effects of increasing noise), we were unable to visually identify which signal was symmetrical and which was not.

Other observations are as follows:

1. PM for the true solution was the highest among the combinations.

2. TWHH was not the lowest for the test involving the 20–200 Hz source signal; the lowest was in the two-possibility combination set B (20–70 Hz).

3. After classification by SR, PM can be used to reinforce identification of the true solution.

F. DISCUSSION

Throughout our tests, we observed that the TRM process was able to produce a focus with the various input geoacoustic parameters tested. This robustness with respect to the mismatch in environmental parameters underlies the applicability of TRM to solve the inverse problem. The location of the focus and its proximity to the true position varies according to whether the parameters were matched or mismatched. The number of ambiguous solutions increased when there were greater numbers of geoacoustic parameters under consideration. It also increased when the grid search was conducted at finer steps.

RD was efficacious as the first metric to narrow all tested combinations to a list of possible solutions. PT appeared less effective (when applied for selection after RD), but this was likely due to the overlapping efficacy of RD and PT. Before embarking on our tests and evaluations, we had hypothesized that PT would be a very good metric. Based on our definition and calculation of SR, however, we had incorporated PT within: if the signal does not peak at zero time, SR will be very high due to the asymmetry. This made PT redundant. SR was extremely selective in identifying the true solution from the possibilities, and for all the tests, SR was the lowest for the true solution. In the noisy environments, however, there was a decreasing contrast between values from matched and mismatched parameters as noise was increased.

We propose for PM to be utilized less as a main metric for classification, and more as a tiebreaker, or for confirmation of the true solution. This was inferred from the lack of consistent performance by the metric in the fine-grid search test. There was also the issue of low contrast in values when comparing matched and mismatched parameters. Using PM as a tiebreaker could be essential when SR encounters challenges in noisy environments. We noted PM performed more consistently than TWHH: in all the seabed with sediment layer models, both with and without added noise, PM was highest for the true solution.

When the TRM process is inputted with a signal of wider bandwidth, it produces a tighter focus, both spatially and temporally. This was evident in Figures 3 and 8 respectively, where two signals of different bandwidths were contrasted. We continued conducting our tests with two signals, one with a wider bandwidth (20–200 Hz) and another with a narrower bandwidth (20–70 Hz). We observed that the signal with the wider bandwidth generally produced higher numbers of ambiguous solutions when RD was applied, especially when brought about by a finer grid search. This was a consequence of the finer resolution brought about by broadband input and, even though more possibilities were observed, the various metric values showed more contrast between matched and mismatched parameters with the signal with wider bandwidth.

In the homogeneous fluid bottom models, SR performed significantly better with the wider broadband signal. When a sediment layer was introduced into the seabed, this advantage was no longer present. Other metrics performed equally well with signals of either bandwidth. There were similar contrasts between metric values when comparing combinations with matched and mismatched geoacoustic parameters.

After we analyzed our results, we propose that in solving the inverse problem and obtaining the true solution, the metrics would be most efficiently utilized in the following recipe, consecutively in the following order:

1. RD
2. SR
3. PM, as verification if necessary

When grid search is employed, we also propose to apply our recipe on a coarse grid search to first narrow down the vicinity of the true solution. This is to be followed with a fine grid search to obtain the accurate values of the geoacoustic parameters. This will optimally balance computation time and accuracy of the parameters. While discussed here in the context of grid search, our recipe is not tied to any particular search technique and is expected to be equally effective with more advanced optimization techniques, such as genetic algorithm.

V. CONCLUSION

A. SUMMARY AND CONCLUSIONS

There are various inverse problems that can be solved with time-reversal mirror (TRM), one of which is characterizing the underwater environment as researched for this thesis. Another important application of solving an inverse problem with the TRM process is the detection of underwater contacts, especially quiet targets, surreptitiously using received noise. To do that, with the correct environment parameters derived and inputted, the similar TRM process can then be used on a signal of interest to find its focus, localizing it and obtaining the location of the source of that signal.

The application of TRM in these two scenarios, first to obtain the unknown parameters of the ocean and second to localize and track a target, has enormous potential in the underwater battlespace. We also concentrated on the single-element TRM for the advantages it provides in naval applications, as a single receiver is more suitable to deploy than a vertical array of receivers.

In solving our inverse problem of characterizing the underwater environment with the concept of TRM as a signal processing technique, we demonstrated ambiguity in the solutions when only a single criterion of spatial focus was used. To be able to isolate the true solution from the range of possibilities became paramount. We hypothesized that a unique solution can be obtained by introducing additional selection criteria, investigated suitable metrics, and tested them in numerical simulations.

Based on expected properties of focus in the back-propagated field with our physics-motivated data processing technique, we identified additional metrics on the basis of the TRM signal's temporal focus, specifically accuracy, compactness, and symmetry. We also expected magnitude of the signal to be suitable.

We conclude that in the bid to obtain the true solution accurately and efficiently, the best performing metrics are as follows, to be applied in the following sequence:

1. Range Discrepancy, the range between the TRM-processed focus and true location

2. Symmetry Ratio (SR), characterizing the symmetry of the TRM-processed signal

3. Peak Magnitude, representing the acoustical pressure at the TRM-processed focus, as verification if necessary

B. RECOMMENDATIONS FOR FUTURE RESEARCH

With our formulation of the metric SR, we observed possible improvements to enhance its performance. One possibility is to fine-tune the calculation, to focus on the vicinity of the main peak rather than the entire TRM-processed signal. This should suppress the effects of noise on the symmetry and provide greater contrast between values from matched and mismatched geoacoustic parameters.

Most importantly, the sequence of applying these metrics, our recipe, is ready for verification with real world data, to demonstrate its robustness and efficiency in identifying the true parameters from possible solutions.

LIST OF REFERENCES

[1] D. R. Dowling and K. G. Sabra, "Acoustic remote sensing," *Ann. Rev. Fluid Mechanics 2015*, vol. 47, pp. 221–243, Jan. 2015. [Online]. https://doi.org/10.1146/annurev-fluid-010814-014747

[2] F. B. Jensen, W. A. Kuperman, M. B. Porter and H. Schmidt. *Computational Ocean Acoustics*, 2nd ed. New York, NY, USA: Springer, 2011

[3] A. Parvulescu and C. S. Clay, "Reproducibility of signal transmission in the ocean," *Radio Electron. Eng.*, vol. 29, no. 4, pp. 223–228, Apr 1965. [Online]. https://doi.org/10.1049/ree.1965.0047

[4] W. A. Kuperman, W. S. Hodgkiss, H. C. Song, T. Akal, C. Ferla, and D. Jackson, "Phase conjugation in the ocean: Experimental demonstration of an acoustic time-reversal mirror," *J. Acoust. Soc. Am.*, vol. 103(1), pp. 25–40, Jan 1998. [Online]. https://doi.org/10.1121/1.423233

[5] O. A. Godin, B. G. Katsnelson, J. Qin, M. G. Brown, N. A. Zabotin, and X. Zang, "Application of time reversal to passive acoustic remote sensing of the ocean," *Acoust. Phys.*, vol. 63, no. 3, pp. 309–320, May 2017. [Online]. https://doi.org/10.1134/S1063771017020038

[6] J. Qin, B. Katsnelson, O. Godin and Z. Li, Geoacoustic inversion using time reversal of ocean noise," *Chin. Phys. Lett.*, vol. 34, no. 9, pp. 094301, Sep 2017. [Online]. https://doi.org/10.1088/0256-307X/34/9/094301

[7] R. M. McMullin, "Application of time reversal to passive acoustic characterization of the ocean," M.S. thesis, Dept. of Phy., NPS, Monterey, CA, USA, 2019. [Online]. Available: http://hdl.handle.net/10945/64026

[8] A. B. Coppens. "An introduction to the parabolic equation for acoustic propagation," Naval Postgraduate School, Monterey, CA, USA, Rep. NPS61-83-002, 1982. [Online]. Available: https://nps.primo.exlibrisgroup.com/permalink/01NPS_INST/ofs26a/alma991005397990603791

[9] M. Dzieciuch, "RAM Parabolic Equation Code, Matlab Style." Accessed April 2, 2021. [Online]. Available: http://staff.washington.edu/dushaw/AcousticsCode/RamMatlabCode.html

[10] M. D. Collins, Naval Research Laboratory, "User's guide for RAM versions 1.0 and 1.0p," unpublished.

[11] B. E. Anderson, M. Griffa, C. Larmat, T. J. Ulrich, P. A. Johnson, "Time reversal," *Acoust. Today*, vol. 4, pp. 5–16, Jan 2008. [Online]. https://doi.org/10.1121/1.2961165

THIS PAGE INTENTIONALLY LEFT BLANK

INITIAL DISTRIBUTION LIST

1. Defense Technical Information Center
   Ft. Belvoir, Virginia

2. Dudley Knox Library
   Naval Postgraduate School
   Monterey, California